

TKK Dissertations 23
Espoo 2006

**GROWTH AND MODIFICATION OF PLANAR AND SELF-
ASSEMBLED SEMICONDUCTOR NANOSTRUCTURES**

Doctoral Dissertation

Jaakko Sormunen



**Helsinki University of Technology
Department of Electrical and Communications Engineering
Optoelectronics Laboratory**

TKK Dissertations 23
Espoo 2006

GROWTH AND MODIFICATION OF PLANAR AND SELF- ASSEMBLED SEMICONDUCTOR NANOSTRUCTURES

Doctoral Dissertation

Jaakko Sormunen

Dissertation for the degree of Doctor of Science in Technology to be presented with due permission of the Department of Electrical and Communications Engineering for public examination and debate in Large Seminar Hall of Micronova at Helsinki University of Technology (Espoo, Finland) on the 10th of March, 2006, at 12 noon.

**Helsinki University of Technology
Department of Electrical and Communications Engineering
Optoelectronics Laboratory**

**Teknillinen korkeakoulu
Sähkö- ja tietoliikennetekniikan osasto
Optoelektroniikan laboratorio**

Distribution:

Helsinki University of Technology
Department of Electrical and Communications Engineering
Optoelectronics Laboratory
P.O. Box 3500
FI - 02015 TKK
FINLAND
URL: <http://atomi.hut.fi/>
Tel. +358-9-451 3121
Fax +358-9-451 3128
E-mail: jaakko.sormunen@tkk.fi

© 2006 Jaakko Sormunen

ISBN 951-22-8037-X
ISBN 951-22-8038-8 (PDF)
ISSN 1795-2239
ISSN 1795-4584 (PDF)
URL: <http://lib.tkk.fi/Diss/2006/isbn9512280388/>

TKK-DISS-2103

Otamedia Oy
Espoo 2006



HELSINKI UNIVERSITY OF TECHNOLOGY P. O. BOX 1000, FI-02015 TKK http://www.tkk.fi		ABSTRACT OF DOCTORAL DISSERTATION	
Author Jaakko Sormunen			
Name of the dissertation Growth and modification of planar and self-assembled semiconductor nanostructures			
Date of manuscript 30th January 2006		Date of the dissertation 10th March 2006	
<input type="checkbox"/> Monograph		<input checked="" type="checkbox"/> Article dissertation (summary + original articles)	
Department Department of Electrical and Communications Engineering			
Laboratory Optoelectronics laboratory			
Field of research Nanotechnology			
Opponent(s) Professor Werner Seifert			
Supervisor (Instructor) Docent Markku Sopanen			
Abstract <p>The epitaxial growth and modification of planar and self-assembled compound semiconductor nanostructures is studied. Quantum dot (QD), quantum ring (QR), and quantum well (QW) structures are grown by metalorganic vapor phase epitaxy. The surface morphology of the samples and nanostructure properties are studied by atomic force microscopy. Photoluminescence (PL) spectroscopy is used to characterize the optical properties of the structures.</p> <p>A novel method for transforming self-assembled InAs islands on InP into QRs is developed. The fabrication of self-assembled semiconductor QRs relies typically on the partial capping of islands to induce the dot-to-ring transformation. In this work, the change in the morphology is achieved without capping, by annealing as-grown InAs/InP islands in a phosphorus-rich flow. With this method, 6–10-nm-high rings are achieved.</p> <p>It is also demonstrated that InGaAs(P)/InP strain-induced quantum dots (SIQDs) can be realized using InAs stressor islands. To adjust the depth of the strain-induced lateral confinement potential, the height of the islands is modified by varying the growth conditions. Furthermore, by varying the composition of the nearly-lattice-matched InGaAsP/InP QW, the SIQD ground state emission wavelength is tuned from 1.3 to 1.7 μm. Luminescence from the excited states in the SIQDs is also observed. The redshift of the SIQD ground state transition from the QW PL peak increases up to 67 meV as the distance between the SIQD and the stressor is reduced to 4 nm. Simultaneously, the luminescence intensity of the SIQD peaks reduces notably. Time-resolved PL measurements reveal that the intensity reduction is accompanied by a faster decay in the carrier populations of the SIQD states. It was concluded that this is due to electron capture to the InAs stressor or surface states associated with it.</p> <p>Finally, the growth of GaN layers for the surface passivation of GaAs is investigated. The passivation effect is probed by PL measurements of near-surface InGaAs/GaAs QWs. The luminescence intensity of samples passivated with GaN is clearly enhanced as compared to unpassivated samples. This shows that the growth of a thin epitaxial GaN layer is an effective means of <i>in situ</i> surface passivation of GaAs.</p>			
Keywords nanotechnology, epitaxy, compound semiconductor, quantum well, quantum dot, quantum ring			
ISBN (printed) 951-22-8037-X		ISSN (printed) 1795-2239	
ISBN (pdf) 951-22-8038-8		ISSN (pdf) 1795-4584	
ISBN (others)		Number of pages 116	
Publisher TKK Optoelectronics Laboratory			
Print distribution TKK Optoelectronics Laboratory			
<input checked="" type="checkbox"/> The dissertation can be read at http://lib.tkk.fi/Diss/2006/isbn9512280388/			

Preface

The work for this thesis has been carried out at the Optoelectronics Laboratory of Helsinki University of Technology during 2002–2005. I would like to express my gratitude to Professor Turkka Tuomi and Professor Harri Lipsanen for the opportunity to work in the laboratory.

I am indebted to Docent Markku Sopanen, the supervisor of this thesis, for his continuous support and interest in my work as well as for his help with the manuscripts. Moreover, I want to thank Juha Riikonen for the fruitful collaboration in the studies of nanostructures. I am also grateful for the valuable cooperation of Dr. Juha Toivonen, Dr. Teppo Hakkarainen, Marco Mattila, Hannu Koskenvaara, and Jouni Tiilikainen. In addition to their input, this thesis would not be the same without the help and good cheer from all the personnel of the Laboratory.

I am most grateful to the Graduate School of Electronics Manufacturing and Tekniikan edistämissäätiö for their financial support.

I especially want to thank my parents Pirkko and Heikki and my sister Suvi as well as my girlfriend Outi for their constant support and encouragement. Finally, huge thanks to all my friends, both terrestrial and airborne.

Espoo, January 2006

Jaakko Sormunen

Table of Contents

Preface	i
Table of Contents	ii
List of Publications	iv
Author's contribution	v
1 Introduction	1
2 Fabrication and characterization of III-V semiconductor nanostructures	4
2.1 Metalorganic vapor phase epitaxy	4
2.2 Fundamentals of self-assembled growth	6
2.3 Atomic force microscopy	9
2.4 Optical spectroscopy	10
3 InAs(P)/InP quantum rings	12
3.1 Self-assembled quantum rings	12
3.2 Fabrication of quantum rings on InP	15
3.3 Evolution of InAs islands into quantum rings	18
4 InP-based strain-induced quantum dots	23

4.1	Strain-induced quantum dots	23
4.2	Fabrication of InGaAs(P)/InP SIQDs	26
4.3	Modification of InAs stressor islands	30
4.4	Optical properties	33
5	Surface passivation of GaAs by GaN	40
6	Summary	44
	References	46

List of Publications

This thesis consists of an overview and of the following publications which are referred to in the text by their Roman numerals.

- I** J. Sormunen, J. Riikonen, M. Mattila, J. Tiilikainen, M. Sopenan, and H. Lipsanen, *Transformation of self-assembled InAs/InP quantum dots into quantum rings without capping*, Nano Letters **5**, 1541–1543 (2005).
- II** J. Sormunen, J. Riikonen, T. Hakkarainen, M. Sopenan, and H. Lipsanen, *Evolution of Self-Assembled InAs/InP Islands into Quantum Rings*, Japanese Journal of Applied Physics **44**, L1323–L1325 (2005).
- III** J. Sormunen, J. Riikonen, M. Mattila, M. Sopenan, and H. Lipsanen, *Modified self-assembly of InAs islands acting as stressors for strain-induced InGaAs(P)/InP quantum dots*, Nanotechnology **16**, 1630–1635 (2005).
- IV** J. Riikonen, J. Sormunen, M. Mattila, M. Sopenan, and H. Lipsanen, *InGaAs/InP Quantum Dots Induced by Self-Organized InAs Stressor-Islands*, Japanese Journal of Applied Physics **44**, L518–L520 (2005).
- V** J. Riikonen, J. Sormunen, H. Koskenvaara, M. Mattila, M. Sopenan, and H. Lipsanen, *Highly Tunable Emission from Strain-Induced InGaAsP/InP Quantum Dots*, Japanese Journal of Applied Physics **44**, L976–L978 (2005).
- VI** H. Koskenvaara, J. Riikonen, J. Sormunen, M. Sopenan, and H. Lipsanen, *Carrier dynamics in strain induced InGaAsP/InP quantum dots*, accepted for publication in Physica E.
- VII** J. Sormunen, J. Toivonen, M. Sopenan, and H. Lipsanen, *Morphology of ultra-thin cubic GaN layers on GaAs(100) grown by MOVPE with DMHy as nitrogen source*, Applied Surface Science **222**, 286–292 (2004).
- VIII** J. Riikonen, J. Sormunen, H. Koskenvaara, M. Mattila, M. Sopenan, and H. Lipsanen, *Passivation of GaAs surface by ultrathin epitaxial GaN layer*, Journal of Crystal Growth **272**, 621–626 (2004).

Author's contribution

The author has written the manuscripts for publications I, II, III, and VII, and he has contributed to the data analysis and manuscripts for publications IV, V, VI, and VIII. The author has especially focused on the fabrication of quantum rings and the growth aspects of self-assembled strain-induced quantum dot structures.

The sample structures and growth parameters for all of the publications were designed by the author and the co-authors. The author has grown the samples for publications I, II, and VII. The samples for publications III, IV, V, VI, and VIII were grown by the author and J. Riikonen.

The atomic force microscopy studies for all the publications were performed by the author.

For publication II, the photoluminescence measurements were carried out by the author. For the rest of the publications, the photoluminescence measurements were performed by J. Riikonen and H. Koskenvaara with help from the author.

1 Introduction

Modern planar fabrication technologies have enabled the realization of layer structures for electronic and optoelectronic compound semiconductor devices with nanoscale dimensions in the growth direction. Prominent examples of this are quantum well (QW) devices, e.g., lasers for fiberoptic communications and optical memory applications as well as high-brightness light emitting diodes for illumination. However, one of the key challenges in the development of novel devices has been achieving nanoscale carrier confinement in all three dimensions. Quantum dots (QDs) behave as zero-dimensional objects, “artificial atoms”, and their energy spectrum consists of discrete levels instead of bands. This property can be utilized in improving the performance of conventional planar devices. Furthermore, completely new innovations such as single-photon light sources [1] for quantum cryptography can be realized. Advanced lithographic techniques can be used to imprint lateral features in the length scale of few tens of nanometers. Thus, by patterning planar structures, it is possible in principle to fabricate quantum dots. However, this approach is time-consuming, and the complex process steps introduce defects into the structure, thus hindering device performance.

During the last fifteen years, self-assembled growth has revolutionized the quantum dot research. The so-called coherent Stranski-Krastanov growth of self-assembled islands can be performed using conventional planar epitaxial techniques. The process can yield a high density of defect-free quantum dots, and the growth of the whole device structure can take place in a single growth run. An example of the device applications is the quantum dot laser [2]. Typically, QD devices consist of self-assembled islands buried in a barrier material with a larger band gap.

An alternative way to create QDs, however, is to use the self-assembled islands as stressors [3]. The tensile strain underneath the islands is utilized to locally reduce the band gap of a near-surface quantum well. The resulting lateral confinement potential is nearly parabolic for both electrons and holes,

and the vertical confinement is achieved by the high-quality interfaces of the QW. The versatility of this approach is that the emission wavelength of the strain-induced quantum dots (SIQDs) can be tuned by adjusting the QW composition, virtually independently of the stressor islands. Furthermore, SIQDs provide an interesting means to study the physics of nearly-perfect quantum dots [4], especially as the strain and the induced confinement potential can be modeled in a straightforward manner [5].

An additional benefit of self-assembled growth is that the shape of the quantum dot island can be controlled. In the case of ring-shaped nanostructures, i.e., quantum rings (QRs), the change in geometry leads to fundamental changes in the electronic properties. As non-simply connected quantum structures, QRs confine carriers into ring-shaped quantum states. Interaction with a magnetic field affects these electronic states and can lead to electronic interference phenomena and persistent currents [6]. In recent years, semiconductor QRs have attracted growing research interest, both for the study of fundamental physics and for potential device applications.

In this thesis, the fabrication of compound semiconductor nanostructures was studied. The modification of planar and low-dimensional structures by epitaxial means was investigated in particular. The main focus of the work was on the self-assembled growth of InP-based QRs and SIQDs. The sample structures were grown by metalorganic vapor phase epitaxy. The morphology of the samples was studied by atomic force microscopy. Photoluminescence spectroscopy was used to characterize the optical properties of the structures.

In publications I and II, the growth and properties of quantum rings were investigated. A novel method for transforming self-assembled InAs islands on InP into quantum rings was developed. In publications III–VI, strain-induced quantum dots were studied. The fabrication of InGaAs/InP quantum dots induced by self-assembled InAs islands was introduced in publication IV. The confinement properties and luminescence wavelength of InGaAs(P)/InP SIQDs were tailored in publications III and V by modifying the stressor islands and other structural parameters. In publication VI, the carrier dynamics in InGaAsP/InP SIQDs were studied by time-resolved photoluminescence. Surface effects related to the InAs stressors and wetting layer were found to influence the carrier recombination in the SIQDs. Finally, the growth of ultrathin epitaxial GaN layers for the surface passivation of GaAs was studied in publications VII and VIII. The luminescence intensity of GaN passivated InGaAs/GaAs near-surface QWs was enhanced

by up to almost three orders of magnitude as compared to unpassivated samples.

The structure of this overview is as follows. The growth and characterization methods used in this thesis are discussed in chapter 2. The fabrication of InAs(P)/InP quantum rings is discussed in chapter 3 summarizing the results from publications I and II. The results from publications III–VI are presented in chapter 4 which discusses InP-based SIQDs. The results from publications VII and VIII, discussing the growth of GaN on GaAs, are presented in chapter 5. The main results of this thesis are summarized in chapter 6.

2 Fabrication and characterization of III-V semiconductor nanostructures

This chapter introduces the fabrication and characterization methods utilized in this work. Section 2.1 outlines the main features of metalorganic vapor phase epitaxy (MOVPE) method used for the growth of the sample structures. Section 2.2 describes the fundamentals of self-assembled growth. The surface morphology of the samples was characterized by atomic force microscopy (AFM) which is introduced in section 2.3. Section 2.4 describes the optical spectroscopy methods.

2.1 Metalorganic vapor phase epitaxy

MOVPE, also known as MOCVD (metalorganic chemical vapor deposition) is based on the use of metalorganic compounds as precursors for the material in epitaxial layers. Since the 1960's, MOVPE has evolved to a widespread technique for the research and industrial production of compound semiconductor thin films. Nowadays, the largest MOVPE reactors can process tens of two-inch wafers in a single growth run. The technique allows the fabrication of sharp interfaces between different materials and precise control of the doping, composition, and homogeneity of the epitaxial layers. The recent fast development of GaN technology relies on MOVPE systems capable of growth at temperatures above 1000 °C and has yielded innovations such as blue and white light emitting diodes (LEDs) [7] and blue lasers [8]. It should also be mentioned that an alternative technique, molecular beam epitaxy (MBE), is commonly used for the fabrication of III-V semiconductor heterostructures [9].

The semiconductor samples for this thesis were grown with a MOVPE system manufactured by Thomas Swan Scientific Equipment Ltd., installed at the Optoelectronics Laboratory in 1993. A schematic diagram of the machine is shown in Fig. 2.1. The metalorganic precursors are located in bubblers which are submerged in baths held at a constant temperature to control the vapor pressure of the precursors. Group III precursors used in this MOVPE system are trimethylgallium (TMGa) for Ga and trimethylindium (TMIn) for In. As group V precursors, tertiarybutylphosphine (TBP), tertiarybutylarsine (TBAs), dimethylhydrazine (DMHy), and trimethylantimony (TMSb) are used for P, As, N, and Sb, respectively. It is worth noting that the group V precursors TBAs [10] and TBP [11] are employed in the system in lieu of the often used arsine (AsH_3) and phosphine (PH_3). Additionally, diethylzinc (DEZn) and disilane (Si_2H_6) are used as dopants for p- and n-type arsenides and phosphides, respectively.

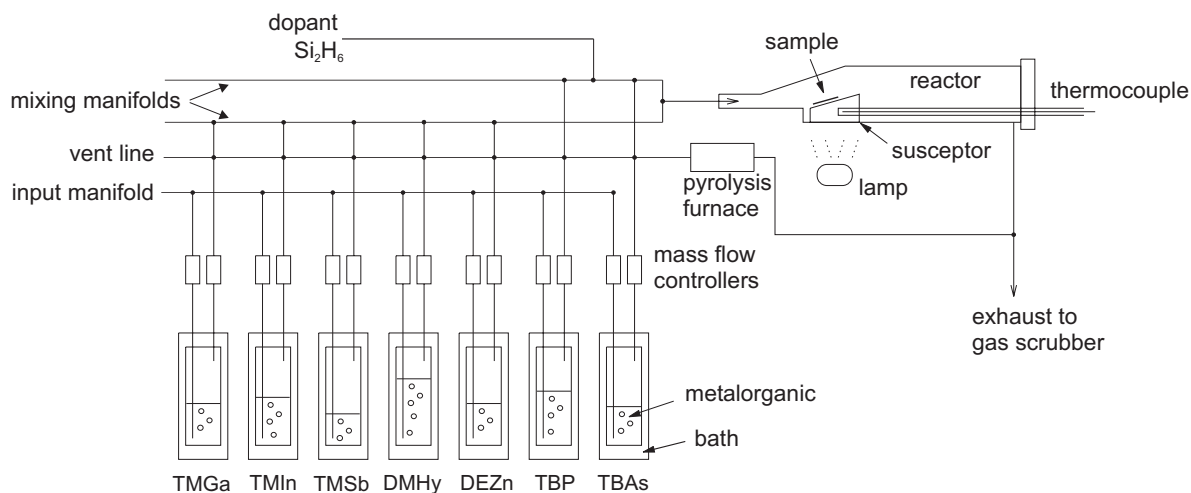


Figure 2.1. Schematic diagram of the MOVPE apparatus.

When carrier gas, typically hydrogen, is led through the bubbler, it is saturated with the vaporized precursor molecules. The gas flows are controlled with mass flow controllers (MFCs). The saturated flow from each bubbler is directed either to the vent line or to the mixing manifold which leads to the reactor. During growth runs, the desired metalorganics are switched by a computer to the reactor to achieve growth of epitaxial layers. By adjusting the gas flows and switching times, the thickness and composition of the layers can be controlled. The total gas flow through the mixing manifolds and the reactor is about 5.5 standard liters per minute which corresponds to a gas flow velocity of roughly 18 cm/s in the reactor. In this work, the growth runs were performed at atmospheric pressure (760 Torr). It is also

possible to grow nanostructures by low-pressure MOVPE at around 50–100 mbar [12]; however, the effect of growth pressure was not investigated in this thesis.

The sample is located in a horizontal quartz-glass reactor on a graphite susceptor. The susceptor is heated by infrared radiation from a halogen lamp. As a result of high temperature, the precursor molecules decompose through complicated pyrolysis reactions and react with the sample surface. Generally, metalorganic molecules start to decompose at 400–500 °C. Therefore, to ensure an efficient use of precursors, MOVPE growth temperatures typically range from 500 to roughly 1200 °C. In the MOVPE system used in this work, the maximum temperature is about 800 °C. The temperature is controlled by a thermocouple inserted in the susceptor. Due to the cooling effect of the gas flow through the reactor, the actual temperature at the sample surface is estimated to be approximately 50 °C lower than the thermocouple reading at 650 °C [13]. All the growth temperatures mentioned in this thesis are thermocouple readings. The gas flow from the reactor, including by-products of the pyrolysis reactions, and the gas flow from the vent line are directed to exhaust where the toxic particles are absorbed and oxidized in a gas scrubber.

The graphite susceptor of the MOVPE apparatus can hold a rectangular sample about 2×2 cm² in size at maximum. A typical sample size in this work was 1×1 cm². The substrates were cleaved from circular wafers 2 inches in diameter. The 001-oriented wafers were semi-insulating single-side polished GaAs (undoped) or InP (Fe-doped). Before the substrates were loaded in the reactor, they were cleaned in an ultrasonic bath first with acetone and then isopropanol. Subsequently, the substrates were rinsed with de-ionized water and blown dry with nitrogen. Prior to the growth of the epitaxial layers, the samples were annealed at 650–700 °C in the MOVPE reactor to remove the thin native surface oxide. The growth rate of the epitaxial layers ranged from 0.2 to 0.4 nm/s depending on the material.

2.2 Fundamentals of self-assembled growth

Strained heteroepitaxy is growth of materials with different lattice constants. The difference in lattice constants introduces strain which can affect the growth process. If the epitaxial film grows pseudomorphically on a lattice-mismatched substrate, the strain energy increases linearly with the layer thickness. After a certain critical thickness, the elastic deformation

energy can be released through dislocation formation. Another route for strain relaxation is the formation of nanocrystals, also known as islands. In the Stranski-Krastanov (SK) growth mode a wetting layer first forms two-dimensionally, after which three-dimensional island growth follows, shown schematically in Fig. 2.2. The driving force behind the formation of islands is the reduction of the total energy of the system, including both the substrate and the epilayer. The thickness of the wetting layer, typically a few monolayers, depends on the materials.

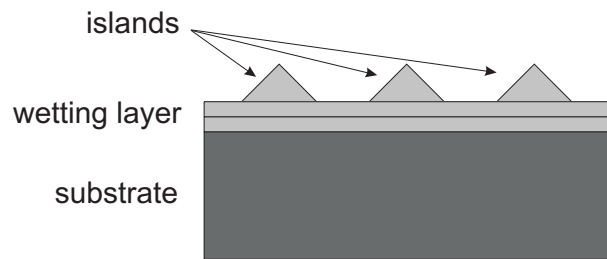


Figure 2.2. Stranski-Krastanov growth mode.

Eaglesham and Cerullo [14] first reported that the initial growth of Ge islands on Si(100) is dislocation-free, dubbing the growth mode coherent SK. The lattice mismatch is partially accommodated by the elastic deformation around the island as shown in Fig. 2.3. The substrate is deformed over a range of approximately $2\times$ the island diameter, and as a consequence, the island is partially relaxed. Examples of other material systems which exhibit coherent SK growth are InGaAs/GaAs [15], InAs/GaAs [16], InGaAs/AlGaAs [17], InP/GaAs [18], InAs/InP [19], and GaSb/GaAs [20]. In all these systems, the epitaxial layer has a larger lattice constant than the substrate and is thus compressively strained.

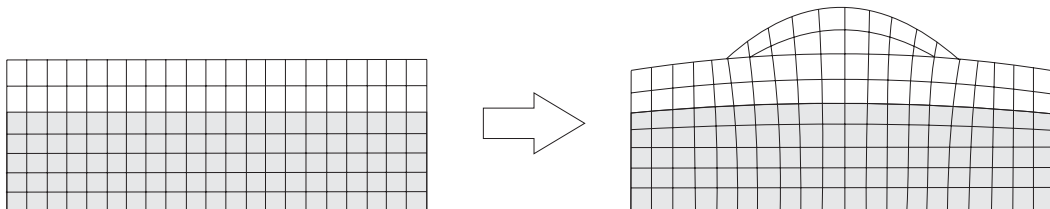


Figure 2.3. Coherent SK island formation and elastic deformation around the island, drawn schematically. The substrate material is marked with light gray.

By optimizing the growth conditions, small coherent (non-dislocated) islands can be fabricated with a high size uniformity and an areal density ranging roughly from 10^8 to 10^{11} cm^{-2} [21, 22]. The islands are typically a few tens of nanometers in diameter and a few nm in height. With a proper choice of materials, the islands can confine carriers in all three dimensions and, hence, are called quantum dots (QDs). Because the formation of the QDs results from the strain-induced morphological transition, i.e., no patterning of the substrate is needed, the growth is often characterized as self-assembled or self-organized.

The growth and properties of self-assembled QDs have been studied extensively. The growth temperature, growth rate, and deposition thickness have been found to influence the size, density and uniformity of the QDs [23–25]. Theoretical studies have shown that these effects can be attributed to the growth kinetics [26, 27]. On the other hand, thermodynamic models have been used to solve the equilibrium shapes of, e.g., Ge islands on Si [28] and InAs QDs on GaAs [29]. There is mounting evidence that to understand the complete picture of the self-assembly of nanostructures, both kinetics and thermodynamics have to be taken into account [30]. For example, indium segregation effects have been shown to control the mass transport in the growth of InAs QDs on GaAs [31].

In the case of InAs QDs grown on InP, arsenic-to-phosphorus (As/P) exchange can have a strong effect on the formation of islands. The unintentional As/P exchange will produce a thicker layer of InAs than would be expected from simple deposition [25, 32]. In the extreme case, InAs QDs have reportedly been achieved on prepatterned InP by As/P exchange alone, without actual InAs deposition [33]. On the other hand, As/P exchange can be used to control the height dispersion and emission wavelength of InAs QDs by exposing the uncapped dots to a phosphorus flux [34, 35]. The exchange effects and QD modification can take place also during the capping process [36].

The electronic states of a QD are discrete and, therefore, QDs can be considered as artificial atoms of a kind. The electronic properties of QDs, e.g., the high density of states, make them promising for use in many device applications, such as the QD laser [2]. Besides being far less sensitive to temperature than conventional quantum well lasers, QD lasers have high differential gain and low threshold current [37]. Recent examples of QD device structures are InAs/InP single photon source emitting near $1.55 \mu\text{m}$, all-optical switch based on state filling in InAs/InP dots [38], and InAs/GaAs QDs for resonant tunneling experiments [39]. Furthermore, InAs/GaAs

QD-based photonic devices operating at $1.3\ \mu\text{m}$, such as a laser capable of digital modulation of up to 12 Gb/s, and a semiconductor optical amplifier (SOA) with high net gain and low chirp have been reported [40].

2.3 Atomic force microscopy

Atomic force microscopy (AFM) is a form of scanning probe microscopy, in which the properties of the sample surface are measured with a probe. In the AFM method, the morphology of the surface is imaged. The method requires very little sample preparation and the measurement can be performed in ambient air. The operating principle of the AFM system used in this work is shown schematically in Fig. 2.4. A sharp silicon nitride probe tip, attached to a cantilever, is brought to a close vicinity of the surface. A laser beam is reflected from the back of the cantilever to a segmented photodiode detector. As the sample is moved laterally by piezoelectric actuators, the microscopic surface features exert atomic Coulombic or van der Waals forces on the tip and cause the cantilever to bend. The bending deflects the laser beam and is detected by the photodiode. A feedback loop provides a correction signal from the detector to the vertical piezoelectric scanner, keeping the laser beam reflection at the same position and thus keeping the force between the probe and the sample constant. A computer gathers the feedback data, converts it into height information and generates an image of the surface features.

The atomic force micrographs in this thesis were taken with a NanoScope E contact-mode AFM. The maximum lateral scan size is $13\times 13\ \mu\text{m}^2$, and the image consists of 512×512 pixels. The vertical resolution of the system can be as good as 0.1 nm, thus resolving height variations of a single monolayer. The lateral resolution, typically a few nm, depends on the shape of the probe and the condition of the surface. Due to the finite curvature of the probe tip, the measured image is a convolution of the surface feature and the tip. The self-assembled nanostructures studied in this work are typically 5–40 nm in height and 100–300 nm in diameter. Therefore, the system can give adequate information on the height, shape, and areal density of these structures.

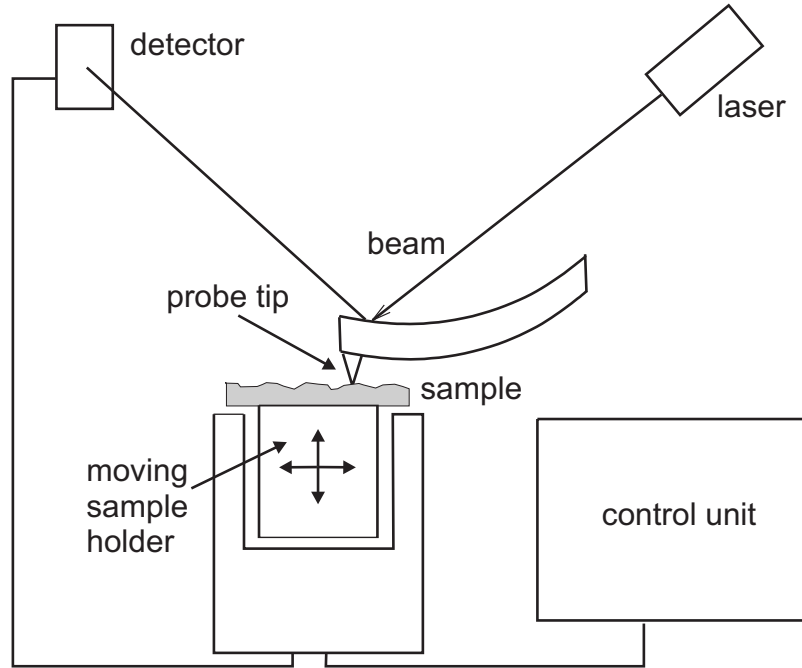


Figure 2.4. Schematic diagram of the AFM setup.

2.4 Optical spectroscopy

The optical properties of the sample structures in this work were characterized by photoluminescence (PL). PL is a commonly used method of optical spectroscopy where carriers (electron-hole pairs) are generated by exciting the sample with photons of sufficient energy. The generated carriers quickly thermalize to the energy states near the band edges or discrete electronic states, and recombine either radiatively or non-radiatively. The spontaneously emitted light is measured, and the emission spectrum is used to identify the electronic structure and different recombination channels of the sample. PL is a non-destructive analysis method and, because the sample is excited optically, no electrical junctions or contacts are needed. Furthermore, with pulsed excitation, PL can give information on the recombination and relaxation mechanisms of the carriers in the time domain.

For the PL measurements in this work, the sample was attached to the cold finger of a closed-cycle helium cryostat and cooled to 10 K. For the continuous-wave measurements, the sample was excited by a laser beam focused to a spot of approximately $200\ \mu\text{m}$ in diameter. Two laser sources were used, either an argon-ion laser emitting at a wavelength of 488 nm or a

diode-pumped frequency-doubled Nd:YVO₄ laser emitting at 532 nm. The luminescence from the sample was dispersed with a monochromator and recorded by a germanium p-i-n photodiode cooled by liquid nitrogen to 77 K. The signal was amplified by a lock-in amplifier connected to a computer for data collection.

The time-resolved PL measurements were performed by exciting the sample with 150 fs pulses from a mode-locked titanium:sapphire laser at the wavelength of 800 nm. The luminescence transients were detected with a cooled microchannel plate photomultiplier and time-correlated single photon counting electronics. The approximate temporal resolution of the system was 30 ps.

3 InAs(P)/InP quantum rings

This chapter discusses the results presented in publications I and II. In these publications, the fabrication of InAs(P) quantum rings (QRs) on InP was studied. First, the properties and fabrication methods of QRs are reviewed in section 3.1. Section 3.2 describes the fabrication and basic characteristics of the QR samples in this work. Section 3.3 discusses the evolution of InAs islands into QRs.

3.1 Self-assembled quantum rings

One of the strengths of the self-assembled growth of low-dimensional quantum nanostructures is that in addition to the size and density, also the shape of the structures can be controlled. A recent example of such control is the self-assembled fabrication of ring-like, or volcano-shaped dots, known as quantum rings. An example of the QR morphology is shown in Fig. 3.1.

Due to their doubly connected geometry, the electronic properties of QRs differ from those of the normal QDs in many respects. The trapping of a single magnetic flux in the interior of a QR can lead to so-called persistent currents associated with a chiral ground state [6]. Especially, quantum interference phenomena related to the Aharonov-Bohm effect [41] have attracted much theoretical and experimental interest [42–44]. Also a high oscillator strength for the ground state transition [45] and a large negative excitonic permanent dipole moment [46] have been reported to distinguish QRs from QDs. The ring-shaped geometry, combined with the magnetic and electronic properties, make QRs interesting candidates for the development of novel devices [47]. In addition to semiconductor QRs, nanoscale rings have also been fabricated from conductive materials, such as gold [48].

The self-assembled growth of semiconductor QRs was first achieved by García et al. by partially capping InAs islands with GaAs [49]. Due to intermix-

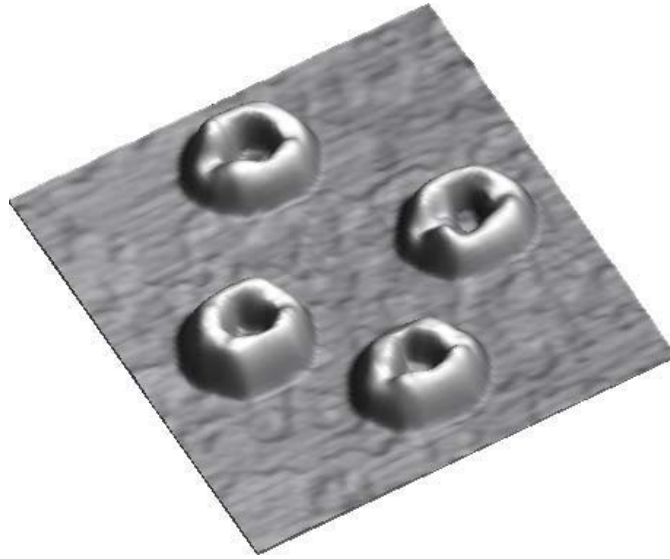


Figure 3.1. AFM image ($1.4 \times 1.4 \mu\text{m}^2$) of InAs(P) quantum rings on InP. The vertical scale is 13 nm [see publ. I].

ing and anisotropic diffusion of In and Ga atoms, the shape of the partially capped islands changes into a crater-like morphology during a growth interruption, as shown schematically in Fig. 3.2. According to a kinetic model of the QR formation [50], In atoms which are more mobile than Ga atoms at typical growth temperatures, diffuse outwards from the initial island location leaving a void. As a result, the outer rims of the QRs consist of an alloyed composition of $\text{In}_x\text{Ga}_{1-x}\text{As}$ [51].

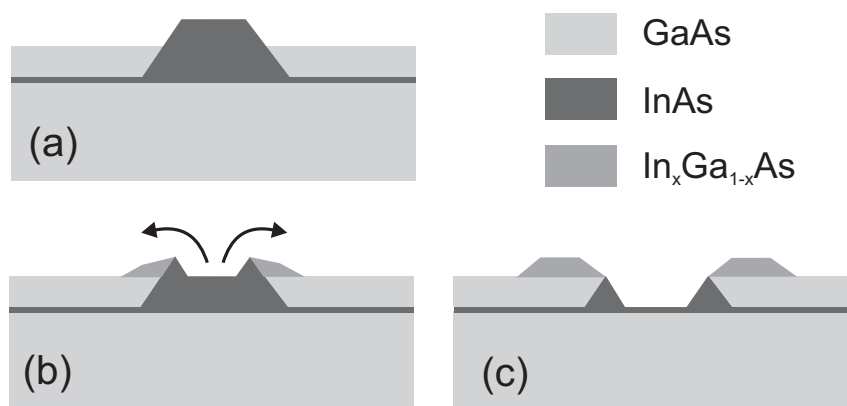


Figure 3.2. Schematic mechanism of the formation of In(Ga)As QRs as a result of partial capping of an InAs island (a) by GaAs. (b) Mobile InAs is diffused outwards, and (c) a void is left in the middle. The figure is based on Refs. [47, 50–52]

A thermodynamic model [52] was later introduced, explaining the ring formation as a surface-free energy equilibrium between the island and the partial capping layer. Further studies [53] have complemented this picture by adding that the mechanism of InGaAs QR formation may involve mobile liquid phases of In and InAs, brought about by the elastic strain energy [31]. The alloying of In and Ga would subsequently form immobile InGaAs [54].

Capacitance-voltage and far-infrared spectroscopy measurements have confirmed that the InGaAs/GaAs QRs confine electrons to ring-like quantum states [6]. As a response to an external magnetic field, the spectra undergo a shift, corresponding to a change in the QR ground state from zero angular momentum into $L = -1$ [51]. PL spectroscopy studies of the electronic interaction in charge-tunable InAs QRs have also been carried out [55].

Very recently, cross-sectional transmission electron microscopy (XTEM) [47] and scanning tunneling microscopy (X-STM) [56] studies on stacked layers of QRs have yielded information on the atomic-scale structure of the In(Ga)As rings. It was reported that the electronic properties of the QR structures are due to the indium-rich crater-like shape, seen as the dark gray area in Fig. 3.2 (c). The larger-radius InGaAs rim (lighter gray) which is made out of the “erupted” material through In–Ga alloying, is typically observed by AFM measurements of the uncapped QR samples. As an application of stacked layers of rings, InGaAs/GaAs QR laser diodes have been demonstrated [57].

In addition to the studies on the electronic and structural properties of QRs, the fabrication methods have attracted great attention. For example, growing an additional AlAs layer on top of the partial GaAs cap was observed to enhance the formation of InGaAs QRs by reducing the surface diffusion of Ga [58]. Although In(Ga)As/GaAs is by far the most studied QR system, other material systems have also exhibited self-assembled QR growth. It is worth noting that the growth mechanisms in these systems differ somewhat from the aforementioned models where both kinetic and thermodynamic argumentation are used.

In a paper [59] where InAs/InP QRs were fabricated by partially capping InAs QDs with InP, the experimental data was reported to disagree with the kinetic model. The difference in group III surface mobilities cannot explain the ring formation as, in contrast to InAs/GaAs QRs, both compounds (InAs and InP) share the same group III atom. Instead, the change in morphology was explained purely by surface-free energy considerations, especially as no compositional change was observed in the QRs.

The effect of elastic strain relaxation on the island-to-ring transformation was brought up in the case of SiGe QRs grown on Si by the partial capping method [60]. It was proposed that Si during the deposition of the partial capping layer diffuses outwards from the top of the partially relaxed Ge QD where the chemical potential for Si adatoms is higher. Simultaneously through surface segregation and diffusion, Ge atoms are released from the QD. They mix and alloy with Si on the QD side surface where the lateral lattice constant matches SiGe with varying composition. XTEM and energy dispersion spectrometry (EDS) measurements [61] have confirmed that substantial intermixing takes place between the Si capping layer and the Ge QD.

As further examples, GaSb/GaAs [62] and CdTe/ZnTe [63] rings have been reportedly achieved by direct deposition. However, the understanding of the formation mechanism in these material systems has not yet fully evolved. Finally, droplet epitaxy has been used to fabricate nearly lattice-matched GaAs/AlGaAs rings [64] and concentric double rings [65]. In the droplet method, the ring formation is explained by GaAs crystallization at the edge of the Ga droplet under As flux.

3.2 Fabrication of quantum rings on InP

Self-assembled InAs quantum dots on InP have been shown to be a promising material system for photonic devices operating around the wavelength range of $1.55 \mu\text{m}$ for fiber optic communications [38, 66]. This, combined with the extraordinary properties of quantum rings (reviewed in the previous section) makes InAs/InP QRs an interesting topic for study. Previously, the height and morphology of InAs QDs have been modified by As/P exchange in order to control their emission energy [34, 35]. In this thesis, As/P exchange was used to transform the InAs QD morphology from dot-like into ring-like.

In publication I, quantum rings were fabricated by annealing as-grown InAs QDs in a phosphorus ambient. Unlike in the typical method used for, e.g., InGaAs/GaAs QRs, no capping of dots was utilized to achieve the change in the QD morphology. The samples were grown on semi-insulating InP(001) wafers. Prior to deposition, the substrates were annealed for 5 min at 650°C after which a 100-nm InP buffer layer was grown at 640°C . The temperature was subsequently decreased to 560°C where 0.6–1.0 monolayers (MLs) of InAs were deposited at a growth rate of 0.8 ML per second. Following the

deposition of InAs QDs, a 10-s flush in TBAs was performed to stabilize the QDs after which the group V precursor flow was switched to TBP. The temperature and duration of the anneal in TBP were varied. A reference uncapped QD sample was also grown where TBAs was not switched to TBP.

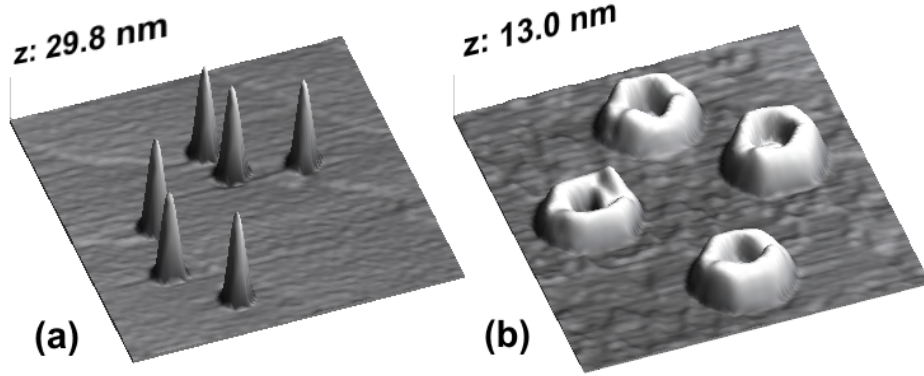


Figure 3.3. Atomic force micrographs of InAs QD samples (a) flushed with TBAs during cooldown and (b) annealed in TBP for 9 seconds at 560 °C. The lateral scale of the images is $1.4 \mu\text{m} \times 1.4 \mu\text{m}$. Note the different vertical scales.

Figure 3.3 (a) shows the AFM image of the reference InAs QD sample. Islands with an average height of 28 nm, a base diameter of 110 nm, and an areal density of $1.8 \times 10^8 \text{ cm}^{-2}$ are observed. For the sample shown in Fig. 3.3 (b), the procedure following the InAs QD growth was different: the sample was annealed for 9 s in TBP at 560 °C after which the temperature was ramped down. The AFM image clearly shows ring-shaped structures (QRs) 8–10 nm in height. The areal density of the islands is $7.2 \times 10^7 \text{ cm}^{-2}$. The differences between the QD and the QR morphology are seen pronouncedly in the AFM cross section profiles in Fig. 3.4. The QR (solid line) has a distinct center hole and the inner and outer diameters are 90 nm and 330 nm, respectively. Comparing to the width of the reference QD (dotted line), it can be noted that most of the QR material has moved outwards from the initial dot location. Based on the AFM data, the volumes of the QD and QR were estimated to be of the same magnitude.

The observed transformation was explained by strain-controlled surface diffusion and As/P exchange. It was already mentioned in section 3.1 that QD strain distribution has been considered to explain the formation of SiGe/Si QRs [60]. Moreover, it has been shown that the chemical potential of partially relaxed, coherent InAs/GaAs islands causes Ga adatom migration away from the QD top surface [67]. Similarly, due to the elastic strain re-

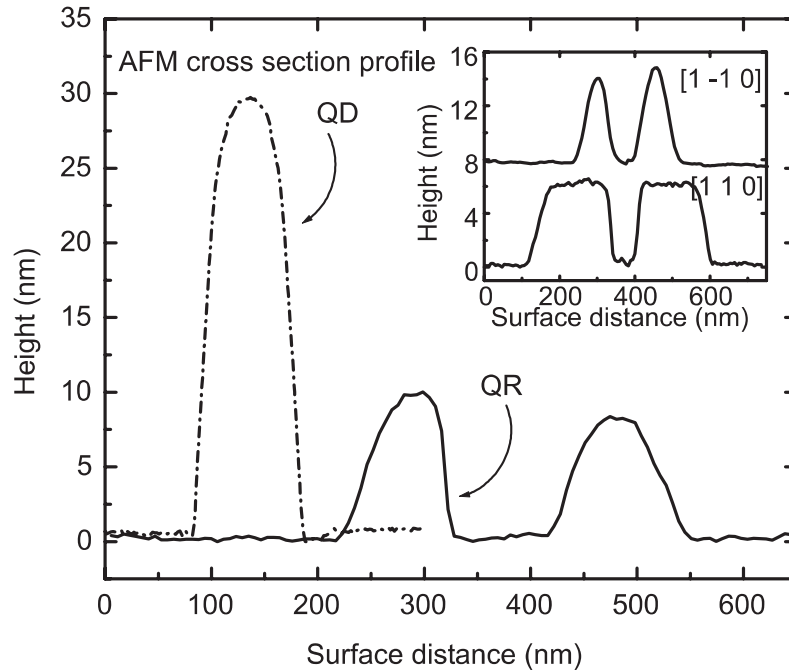


Figure 3.4. AFM cross section profiles, taken along the $[1 -1 0]$ direction, of an InAs QD (dotted line) and a QR (solid line) formed at $560\text{ }^{\circ}\text{C}$. The inset shows corresponding profiles of a QR formed at $540\text{ }^{\circ}\text{C}$, taken along the $[1 -1 0]$ and the $[1 1 0]$ direction. The curves are offset for clarity [publ. I].

laxation, the top of a coherent InAs/InP QD is an energetically unfavorable site for InP growth. Thus, if In adatoms are released from the InAs QD under P overpressure, they would migrate outward along the surface of the island [35]. As a general note, it is acknowledged that In atoms are mobile at typical MOVPE growth temperatures also in the absence of group V exchange effects.

A schematic diagram of the proposed QR formation process is shown in Fig. 3.5. When TBAs is switched to TBP, As/P exchange and As desorption release In atoms from the InAs lattice (a). The In adatoms migrate towards the base of the InAs island where the lateral lattice constant is closer to InP (b), and are re-incorporated at an energetically more favorable site. Material redistribution continues (c) until the initial InAs island has vanished.

It was also observed in publication I that the rate of material redistribution in the dot-to-ring transformation decreases as the temperature is decreased.

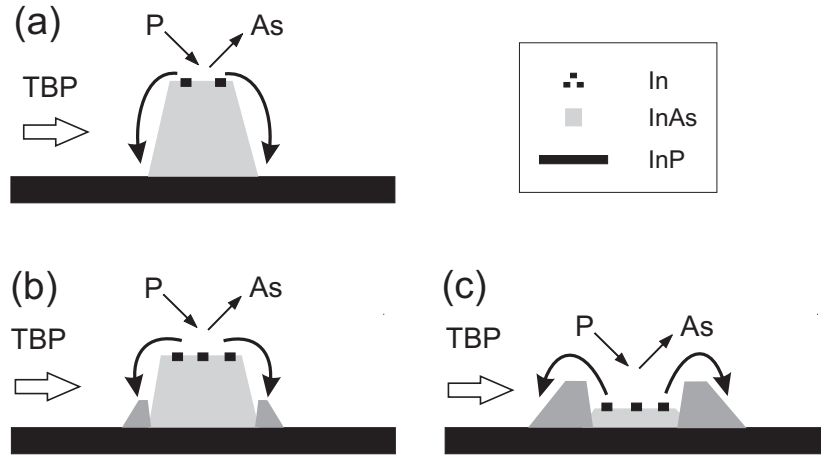


Figure 3.5. Schematic diagram of the dot-to-ring transformation of an InAs/InP QD. (a) In atoms are released by As/P exchange and migrate outwards from the InAs island. (b) In atoms are re-incorporated at the interface of the QD and the flat surface. (c) Material redistribution continues until the initial InAs island has disappeared [publ. I].

With decreasing temperature, both As/P exchange [68] and In surface migration slow down, which might explain the observed trend. Moreover, the rings formed at 540 °C were notably elongated in the $[1\ 1\ 0]$ direction. The elongation is clearly illustrated by the AFM cross section profiles in the inset of Fig. 3.4. All in all, it was noted that the dot-to-ring transformation seems to be dominated by kinetic effects. The mass transportation and strain minimization associated with QR formation is most likely a complex process with both kinetic and thermodynamic characteristics. However, in this case, the pure thermodynamic model which assumes that the QR is formed as the surface energy of the QD with respect to a partial capping layer is minimized, would not offer a plausible explanation.

3.3 Evolution of InAs islands into quantum rings

In publication II, the progression of the QD-to-QR transformation was studied by modifying the growth process introduced in publication I. The temperature and duration of annealing in TBP were varied to yield nanostructures with diverse morphologies. The evolution was observed *ex-situ* by atomic force microscopy and photoluminescence measurements. Following

a similar sample preparation as in publication I, the initial islands were grown at 550 °C by depositing 1.4–1.6 MLs of InAs, yielding an areal island density of around 10^8 cm^{-2} .

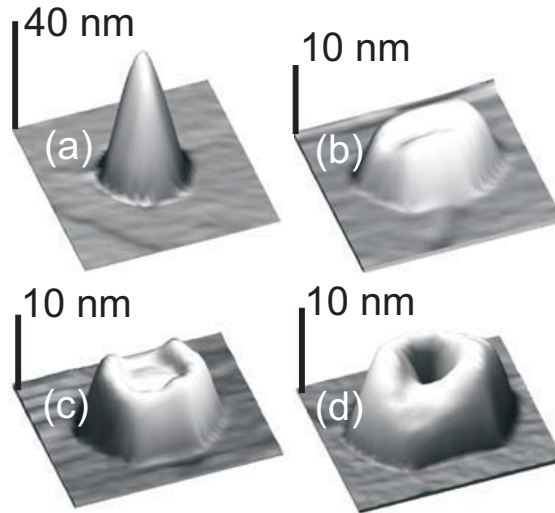


Figure 3.6. Atomic force micrographs ($0.5 \times 0.5 \mu\text{m}^2$) of (a) as-grown InAs island, and islands annealed in TBP at (b) 520, (c) 540, and (d) 555 °C. Note the different vertical scale in (a) [publ. II].

The effect of the annealing temperature on the morphology of the QRs was studied first. After the deposition of InAs, the temperature was ramped down to 400 °C in a TBAs flow to ensure that the initial islands are independent of the annealing temperature. Then, TBP was introduced to the reactor as the temperature was ramped up again. To investigate the progression of the QD-to-QR transformation with increasing temperature, the maximum temperature of the annealing step was varied between 520 and 555 °C. Fig. 3.6 shows AFM images of (a) the as-grown InAs island, and QRs annealed at (b) 520, (c) 540, and (d) 555 °C. Note the larger vertical scale of 40 nm in Fig. 3.6 (a). The height of the island was reduced notably to roughly 10 nm in all the annealed samples. However, a distinct central hole was observed only in the sample of Fig. 3.6 (d) although there was a slight depression already visible in Fig. 3.6 (c).

To study the progression of the morphological transformation with time, another set of QR samples was fabricated at a constant temperature. After the deposition of 1.6 MLs of InAs and a growth interruption in a protective

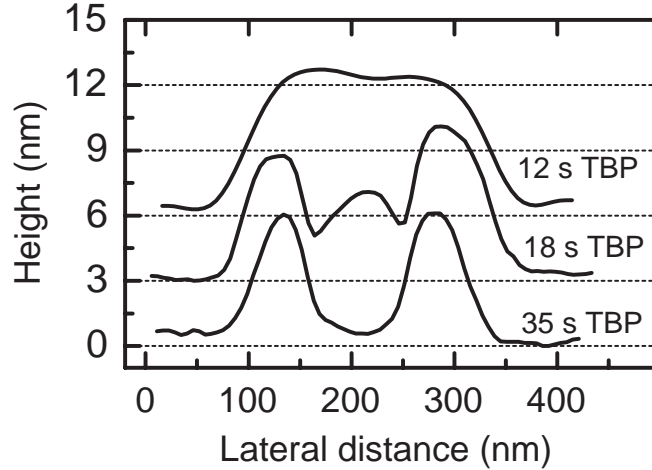


Figure 3.7. AFM cross section profiles of QRs fabricated at $550\text{ }^{\circ}\text{C}$, taken along the $[1\ -1\ 0]$ direction. The profiles are offset vertically for clarity [publ. II].

flow of TBAs, TBP was switched to the reactor while maintaining a temperature of $550\text{ }^{\circ}\text{C}$. The duration of the annealing step was varied between 0 and 35 s before the temperature was ramped down. Fig. 3.7 shows the AFM cross section profiles of individual QRs from samples annealed for 12, 18, and 35 s.

The height of the structures is reduced to around 6 nm in all the samples in Fig 3.7. However, the top of the structure is still mostly flat after a 12-s TBP anneal. After 18 s of annealing, there is a distinct depression in the center of the QR but some material is still remaining in the middle. When the annealing time is 35 s, the central hole extends to the InP buffer surface. Therefore, most of the material from the initial InAs island has been redistributed. The above observations of the material redistribution would seem to suggest that the hole formation is a continuous diffusive process in the case of uncapped InAs/InP QRs. All in all, the QRs grown at a constant temperature are very similar compared to the QRs fabricated by lowering the temperature to $400\text{ }^{\circ}\text{C}$ before the TBP annealing step. The difference in the size of the QRs is explained by the size variation of the initial InAs islands, resulting from the different growth procedures.

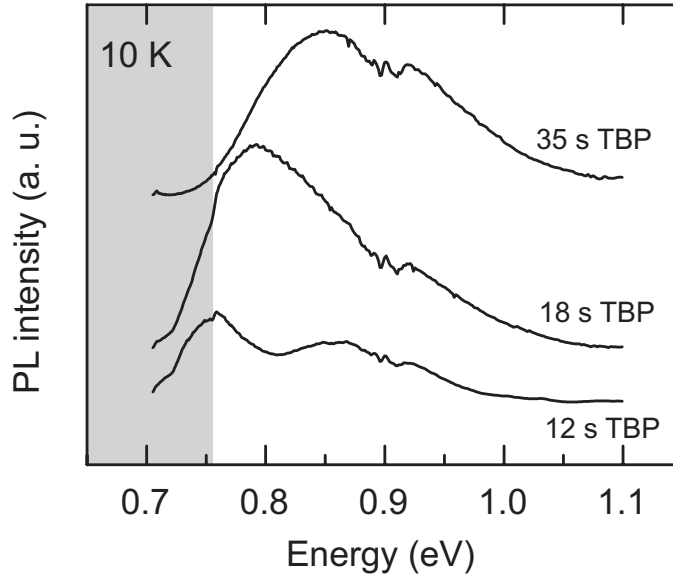


Figure 3.8. Photoluminescence spectra of QR samples annealed in TBP at 550 °C for 12, 18, and 35 s. The gray area on the left represents the response cut-off region of the Ge detector [publ. II].

To study the optical properties of the QRs, samples similar to the previous set were grown with a 20-nm InP capping layer on top of the QRs. Fig. 3.8 shows PL spectra of the samples with a varying duration of TBP annealing. It should be noted that the Ge diode used as the detector cuts off most of the luminescence below 0.75 eV, marked with gray in Fig 3.8. However, it is still clearly seen that there is a blue-shift in the luminescence as the annealing time in TBP is increased from 12 s to 35 s.

It was already noted above that the height of the evolving QRs does not change significantly after 12 s of annealing. Therefore, most of the blue-shift observed in Fig. 3.8 is very likely due to a compositional change in the material as it is redistributed from the initial InAs island. Thus, it is assumed that the broad luminescence around 0.85 eV (top curve) originates from QRs with an undetermined composition of InAsP. Moreover, in the lowest PL curve in Fig. 3.8, a weaker peak is seen around 0.85 eV. It is conceivable that the origin of this peak is a P-rich rim of the evolving QR, whereas the low-energy side luminescence might come from the As-

rich center. As the QD-to-QR transformation proceeds, such short-range compositional variations may be leveled out.

To obtain exact data on the composition of the QRs in different stages of their evolution, studies using, e.g., transmission electron microscopy would be needed. However, in the light of the results presented here, it can be said that As from the initial InAs island is re-incorporated to some extent in the final InAsP QR because the observed luminescence differs from that of pure InP. In contrast to our findings, in a paper where InAs/InP QRs were grown by molecular beam epitaxy (MBE) using a partial capping layer, no compositional change in the QRs was reported [59]. This may be due to the lower growth temperature (495 °C) as compared to this work (550 °C) which would reduce the effects of As/P exchange.

4 InP-based strain-induced quantum dots

This chapter discusses the results presented in publications III, IV, V, and VI. In these publications, InGaAs/InP and InGaAsP/InP quantum dots induced by self-assembled InAs stressor islands were studied. In section 4.1, the concept of strain-induced quantum dots (SIQDs) is introduced as a background for the current work. Section 4.2 describes the fabrication and basic properties of the SIQD samples. The modification of the InAs stressor islands is discussed in section 4.3. The optical properties of the SIQDs are presented in section 4.4.

4.1 Strain-induced quantum dots

Most QD device structures consist of layers of self-assembled islands buried in a barrier material with a larger band gap, such as InAs QDs on GaAs. However, the confinement of carriers can also be achieved by using strain to modulate the band structure of a direct band gap semiconductor. Biaxial strain can shift the conduction band edge and lift the degeneracy of the valence bands. Tensile strain in the growth plane reduces the band gap of III-arsenides and III-phosphides. Kash et al. first demonstrated the lateral strain-induced confinement of carriers in an InGaAs/InP quantum well [69]. A stressor was fabricated on top of the near-surface QW by etching a mesa pillar of compressively strained InGaAsP. The vertical confinement was achieved by the QW while the strain-induced modulation of the QW band edges confined carriers laterally under the InGaAsP mesas.

The fabrication of strain-induced quantum dots was later refined by Sopenan and co-workers who introduced the use of self-assembled InP islands as stressors for InGaAs/GaAs QW [70]. Fig. 4.1 shows the structure of a

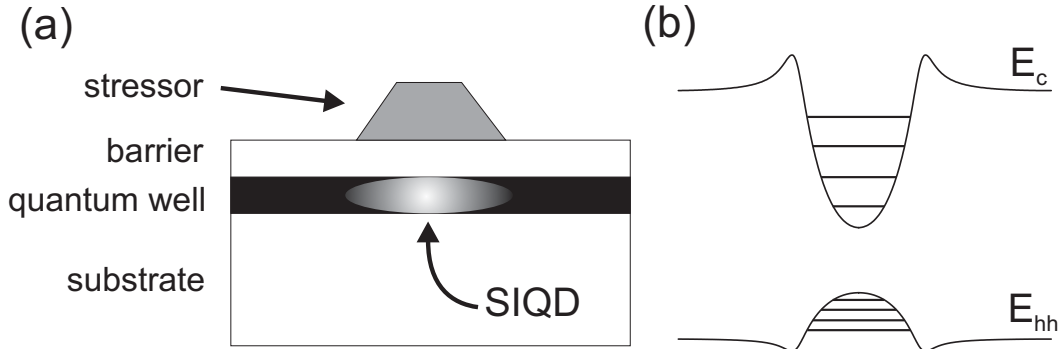


Figure 4.1. (a) Schematic structure of a strain-induced quantum dot sample. (b) Schematic deformation of the quantum well conduction band and heavy hole band in the vicinity of the stressor. The horizontal lines depict the energy levels of quantized electronic states.

SIQD sample and the schematic deformation of the QW band edges. In contrast to conventional buried QDs where the carriers are confined in the self-assembled islands, the SIQD structure confines carriers in the strain-modulated region of the quantum well. The resulting lateral confinement potential is nearly parabolic for both electrons and holes.

The advantage of using self-assembled islands as stressors is that the structure can be grown entirely *in situ*, i.e., no post-growth processing is required. Furthermore, the approach extends the benefit of coherent SK growth in forming quantum-sized dots into materials where direct island growth is unattainable [3]. Conversely, self-assembled islands as QDs lack the flexibility of band gap engineering that quantum wells and hence SIQDs have. As an example of potential applications, a device structure for the storage of photo-generated excitons, based on the coupling of InAs QDs and SIQDs, has been proposed [71].

The depth of the strain-induced confinement potential and the level splitting of the SIQD states can be tailored by adjusting the top barrier thickness or the size of the stressor islands [72]. The emission wavelength of the QDs can also be tuned by adjusting the QW composition. In addition to strain-induced InGaAs/GaAs QDs, self-assembled SIQDs have previously been fabricated using GaInNAs/GaAs [73], GaInP/AlGaInP [74], GaAs/AlGaAs [75, 76], and SiGe/Si [77] QWs. Except for SiGe/Si SIQDs which have been grown on a Si substrate with Ge stressor islands, all of the aforementioned structures have been grown on GaAs substrates. The fabrication of SIQDs

based on InP substrates and utilizing InAs islands as stressors was introduced in publication IV.

Wang et al. have studied the effect of the stressor material on the confinement effect of AlGaAs/GaAs SIQDs [78]. InP stressors (3.8 % lattice mismatch on GaAs) were compared to GaSb stressors (7.8 % mismatch on GaAs). It was observed that choosing a stressor with higher lattice mismatch is not an effective way to increase the strain effect. The higher mismatch was shown to yield smaller self-assembled islands and thus a weaker strain effect. Furthermore, surface states associated with GaSb were found to quench the SIQD PL emission for barrier thicknesses less than or equal to 10 nm. The band gap of InP (1.42 eV) is larger than that of GaSb (0.81 eV) which, combined with the surface passivation effect of InP on GaAs [79], can effectively reduce the surface recombination in the case of InP stressors.

The carrier confinement in SIQD structures can be characterized by photoluminescence. Fig. 4.2 shows PL spectra from an InGaAs/InP SIQD structure, measured at different excitation intensities. The spectrum measured at the excitation of 10 W/cm^2 shows the PL peak from the SIQD ground state (QD0) at 0.78 eV and luminescence from the QW at 0.84 eV. As the intensity is increased to 30 W/cm^2 and further to 100 W/cm^2 , emission from the first excited SIQD state (QD1) can be seen to emerge at 0.79 eV. At higher excitation intensities of 300 W/cm^2 and 1000 W/cm^2 the spectra clearly show three SIQD peaks, and a fourth feature also seems to arise. The level splitting between consecutive energy states is almost equal (14.9–15.5 meV) as a result of the nearly-parabolic confinement potential [5, 80].

The emergence of luminescence from excited states as the excitation intensity is increased (Fig. 4.2) is explained by state filling: an entirely filled state prohibits relaxation from a higher state (Pauli blocking) and the next level starts to populate [3, 4]. However, because the excitation beam has a Gaussian intensity distribution laterally, increasing the excitation level means also that the number of SIQDs participating in the PL increases. Therefore, the intensity of the ground state (and other states) is increased with increasing excitation even if the peak from the next level is already seen. In addition to the continuous-wave characterization of the steady state, time-resolved PL measurements have yielded information on the carrier dynamics in SIQDs. In the case of the InGaAs/GaAs SIQDs, the carrier capture, relaxation, and recombination processes which contribute to the PL behavior have been studied [4, 81–83]. In this thesis, the carrier dynamics in InGaAsP/InP SIQDs were investigated.

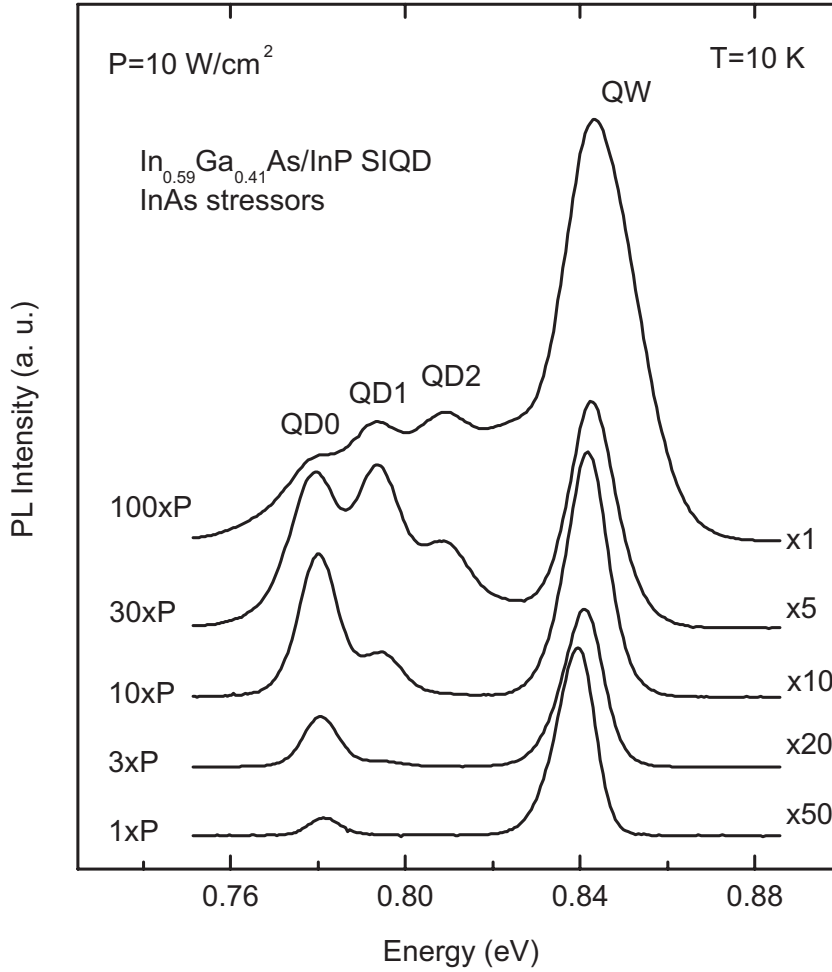


Figure 4.2. PL spectra of an InGaAs/InP SIQD sample measured at different excitation intensities.

4.2 Fabrication of InGaAs(P)/InP SIQDs

It was already mentioned in section 4.1 that strain-induced quantum dot structures have been previously fabricated on GaAs and Si substrates. Because of material constraints, if one wishes to adjust the band gap of the InGaAs/GaAs or SiGe/Si near-surface quantum well, one unavoidably changes also the strain of the structure. This can be a limiting factor in the tunability of the emission properties of the SIQDs. However, if one chooses InP as the substrate, it is possible to fabricate the structure with an InGaAs QW, lattice-matched to InP. Furthermore, the use of a lattice-matched quaternary InGaAsP QW allows a wide tuning range for the wavelength of the

dots. For example, it is possible to span the important telecommunication wavelength regions of 1.3 and 1.55 μm with an InP-based SIQD structure.

The GaAs-based SIQD structures have relied mainly on coherent InP islands as stressors. Obviously, in the case of InP substrate, another material for the stressor island must be found. The lattice mismatch between InAs and InP (3.2%) is close to the mismatch between InP and GaAs (3.8%). Furthermore, the coherent SK growth of InAs islands on InP has been established as a pertinent technique for the fabrication of buried QDs [84]. Therefore, InAs islands were chosen as the stressors in this work. It should be noted though that as the band gap of InAs (0.35 eV) is lower than that of InP, some degree of carrier recombination may take place in the stressors. This issue is addressed in publication VI.

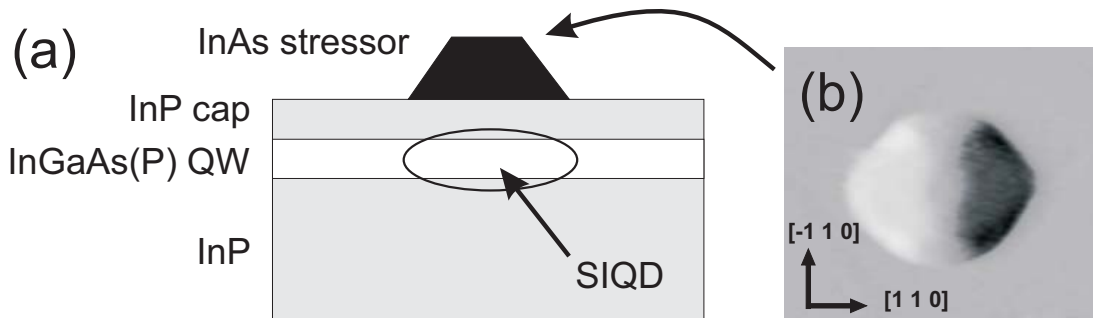


Figure 4.3. (a) Schematic structure of the InGaAs(P)/InP SIQD samples. (b) AFM image ($0.2 \times 0.2 \mu\text{m}^2$) of an InAs stressor island.

The schematic structure of the InP-based SIQD samples, introduced in publication IV, is shown in Fig. 4.3 together with an AFM image of an InAs stressor island having a height of 26 nm and a base diameter of 130 nm. The samples were grown on vicinal InP(001) substrates. To ensure an atomically flat surface, a 100-nm InP buffer was first deposited at 640 $^\circ\text{C}$. The InGaAs(P) quantum well and an InP cap layer (barrier) were subsequently grown, also at 640 $^\circ\text{C}$. The thickness and composition of the QW and the thickness of the capping layer were varied as explained later. The composition of the QWs was determined by PL measurements and high-resolution x-ray diffraction (XRD). For the growth of the stressor islands, the temperature was decreased to 550–570 $^\circ\text{C}$. Island growth was achieved by depositing nominally 0.65–1.7 MLs of InAs. Self-assembled islands are typically grown at a stable temperature. However, in this work InAs was deposited during the first few seconds of a temperature ramp-down from the nominal growth temperature of 550–570 $^\circ\text{C}$ in order to reduce the effects of As/P exchange [35, 85, 86], such as the uncontrolled accumulation of excess material into

the islands after deposition. Compared to growth at a constant temperature [25], this procedure was found to result in more homogeneous islands and is further discussed in section 4.3. In this text, the growth temperature of the islands refers to the nominal temperature before the ramp-down step. Figure 4.4 shows an AFM image of the InAs stressor islands grown at 560 °C and a corresponding island height distribution histogram. The islands have an areal density of $1.2 \times 10^9 \text{ cm}^{-2}$ and an average height of 23.3 nm, and represent one typical stressor island ensemble fabricated in this work.

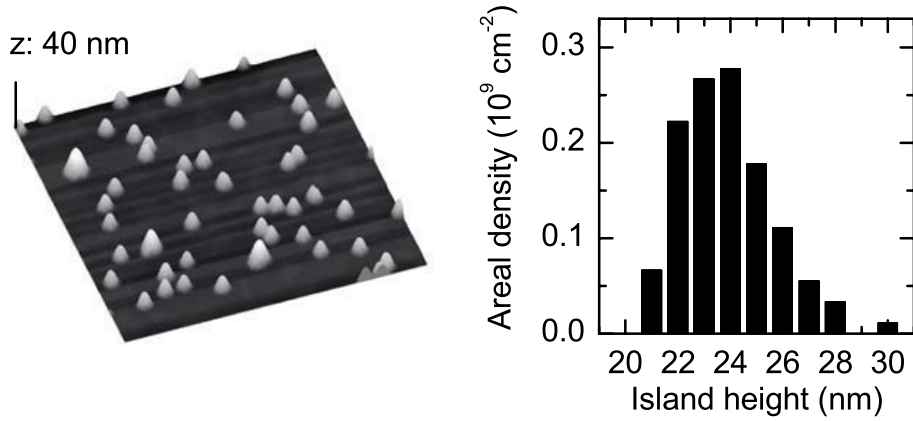


Figure 4.4. (left) AFM image ($2 \times 2 \mu\text{m}^2$) of InAs stressor islands grown at 560 °C and (right) the height distribution histogram of the island ensemble [publ. IV].

In publication III, the strain induced by the InAs stressor in the middle of the quantum well was calculated using the continuum elasticity theory. Assuming a 10-nm-thick $\text{In}_{0.59}\text{Ga}_{0.41}\text{As}$ QW and a 7-nm InP cap, the finite element method (FEM) was used to computationally solve the strain components. To find out the effect of the size of the island on the induced strain, the height of the island was varied from 8 to 40 nm. On the basis of AFM observations, the aspect ratio (height/base diameter) was assumed to be a constant 0.2. Fig. 4.5 shows plots of the total strain in the middle of the $\text{In}_{0.59}\text{Ga}_{0.41}\text{As}$ quantum well under the stressors of different size.

Because the band-edge deformation depends linearly on the strain components, the depth of the lateral confinement potential is proportional to the strain difference between the center of the island and far away from the island. The inset of Fig. 4.5 shows the relative confinement depth as a function of stressor height, normalized to 1 at $h = 24 \text{ nm}$. The confinement depth declines rapidly as the height of the stressor decreases below 15 nm.

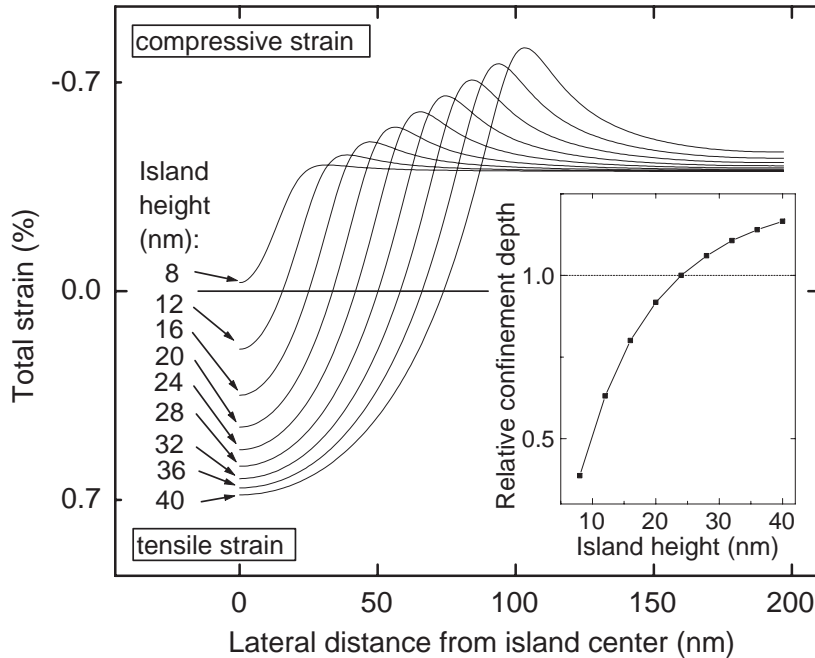


Figure 4.5. Calculated total strain in the InGaAs QW under the InAs stressor island as a function of lateral (radial) distance. The inset shows the relative depth of the lateral confinement potential as a function of island height [publ. III].

Thus, islands much smaller than that are unlikely to induce quantum dots with high quantization. On the other hand, the depth of confinement increases only somewhat above 30 nm. Moreover, at such height, the islands typically become non-coherent via dislocation formation. With the values from the strain calculation for an InAs island 24 nm in height, the quantized energy levels in the SIQD were calculated assuming a 2D rotationally symmetric potential for the lateral confinement. Using $m^* = 0.033m_0$ for electrons and $m^* = 0.049m_0$ for lateral “heavy” holes, a level splitting of 15 meV for consecutive QD transitions was obtained. The calculated redshift of the QD0 ground state transition from the QW ground state was 61 meV of which 49 meV originated from the conduction band side. These values are in good agreement with the experimental results from PL measurements presented in section 4.4.

4.3 Modification of InAs stressor islands

In publication III, the modification of the InAs stressor islands was studied by varying the growth conditions and the sample structure. First, the influence of a compressively strained $\text{In}_{0.59}\text{Ga}_{0.41}\text{As}$ near-surface QW on the self-assembly of the InAs islands was investigated. 1.3 and 1.7 MLs of InAs was deposited both directly on a plain InP buffer (without the QW) and on the capping layer of a near-surface QW. During growth, the temperature was ramped down from 550 °C, as described in section 4.2. For comparison, samples with the QW were also grown at a constant temperature of 550 °C. In Fig. 4.6, the areal density of the islands is plotted as a function of average island height, determined by AFM analysis of the samples. It was observed that the areal density is notably lower for islands grown on plain InP as compared to islands grown on the near-surface QW. On plain InP, a deposition of 1.3 ML seems to be just above the critical limit for island formation. This implies that the threshold for the 2D-3D transition may be lowered in the samples with the QW. Furthermore, by comparing the total material volumes in the dots, it was noticed that islands grown on the near-surface QWs have accumulated more material than the islands grown on plain InP. It is likely that most of the extra material comes from the exposed InP surface through As/P exchange [25] which may be further enhanced by strain [32].

It was also observed that the islands grown at a stable temperature are larger than the islands grown during the temperature ramp-down and, because the areal density remains approximately the same, have accumulated more material. It was concluded that this must be due to a difference in the rate of As/P exchange during the growth of the islands. Group V exchange before the nucleation of the islands affects mainly the nucleation density through an increase in the supersaturation of mobile adatoms on the surface [21]. Therefore, similar island densities imply that the growth conditions before the nucleation are close to identical in the ramp-down process and growth at a constant temperature. However, after nucleation, the ramp-down procedure results in the diminished As/P exchange which is seen as a decrease in the excess material accumulated in the islands. Simultaneously, the full-width at half-maximum (FWHM) of the island height distribution dropped from 3.9 nm to 3.1 nm (at 1.7 ML), as determined in publication III by fitting Gaussian profiles to the island height histogram data. Thus, the homogeneity of the island ensemble was improved, presumably due to a suppression of As/P exchange during the nucleation phase which is thereby shortened.

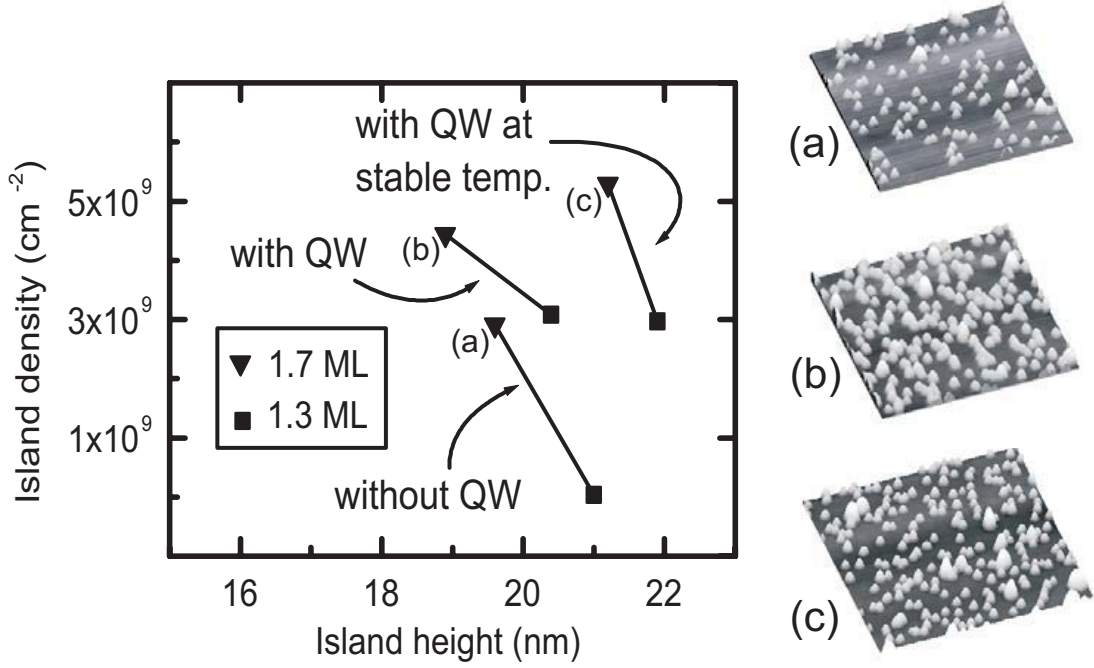


Figure 4.6. Areal density of InAs islands grown on plain InP buffer (without QW), near-surface InGaAs QW, and near-surface QW at a stable temperature, plotted against average island height. On the right, the corresponding $2 \times 2 \mu\text{m}^2$ AFM images (a)–(c) are shown for the deposition of 1.7 MLs.

The average size and areal density of the InAs stressor islands were tuned by varying the growth temperature and the nominal deposition thickness. Fig. 4.7 shows the areal density of InAs islands plotted against average height, as determined from the AFM data. The stressor size is noted to increase with temperature regardless of the deposition thickness. As a general trend, the island density and height are inversely proportional. This is a consequence of mass distribution [12]: because the density of nucleated islands decreases with increasing temperature [21], the deposited material is distributed over fewer islands at higher temperatures. However, with a deposition thickness of 0.65 ML, the InAs island density increases with increasing temperature. This behaviour was explained by acknowledging that the nominally deposited thickness here is well below the critical limit for the 2D-3D transition (up to 3–4 MLs [87]), and the rest of the needed material comes from the interface through As/P exchange. Raising the temperature increases the rate of exchange [85] which in turn amounts to a higher su-

persaturation at the onset of nucleation. Hence, the nucleation density is increased.

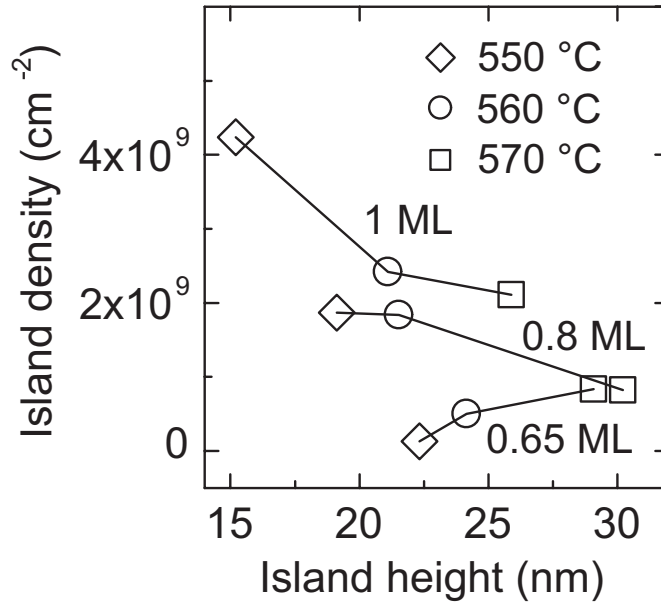


Figure 4.7. Areal density of InAs stressor islands plotted against average height. The figure shows samples grown at 550, 560, and 570 °C with different InAs deposition thicknesses (0.65–1.0 ML) [publ. III].

In addition to affecting the nucleation, the As/P exchange was also shown to affect the growth of the islands. To estimate the amount of incorporated "exchanged" material, the total material volumes in the islands were calculated from the AFM data (not shown here). It was noted that with a fixed deposition thickness raising the growth temperature distinctly increased the volume in the islands. At 570 °C, the material volumes were typically more than twice as high as at 550 °C. Three conclusions were drawn from this: (i) material accumulated from the interface through As/P exchange seems to account to more than half of the material in the islands grown at 570 °C. (ii) With the exchanged (In)As, also some of the released (In)P might be re-incorporated into the islands, thus forming InAsP [12]. This alloying would obviously diminish the strain effect of the stressor. (iii) The effect of excess material accumulation could be drastically reduced by lowering the temperature. However, this would also lead to a reduction in the size of the islands which is an undesired effect. Ideally, the temperature should be high enough during nucleation to ensure a right density of coherent islands but low enough during the subsequent growth of the islands to reduce the

As/P exchange effects. This again motivated the use of the temperature ramp-down during InAs deposition.

4.4 Optical properties

The effect of the stressor size on the confinement effect of the SIQD was studied by PL measurements in publication III. The stressor island distribution was varied as explained in section 4.3. Samples with either an $\text{In}_{0.59}\text{Ga}_{0.41}\text{As}$ or an $\text{In}_{0.68}\text{Ga}_{0.32}\text{As}_{0.83}\text{P}_{0.17}$ QW were studied. In Fig. 4.8, PL spectra from InGaAs and InGaAsP SIQD samples with InAs islands grown at 560°C are shown. At low excitation intensity (dashed lines), both samples mainly show luminescence from the QW and the quantum dot ground state (QD0). In the InGaAs sample, the QD0 peak at 0.733 eV is redshifted by 66 meV from the QW peak. Meanwhile, the InGaAsP QW luminesces at 0.838 eV and the corresponding QD0 peak is redshifted by 61 meV. At a higher excitation intensity (solid lines), both samples show state filling, i.e., luminescence from higher SIQD states (QD1-QD3) emerge as lower states become fully populated [4], [publ. IV]. By fitting Gaussian profiles to the shown spectra, the level splittings between consecutive QD states were resolved to be 14.1–15.0 meV (InGaAs QDs) and 14.7–15.6 meV (InGaAsP QDs). These values are close to the calculated level splitting of 15 meV (section 4.2).

It was already mentioned in section 4.2 that according to computation, increasing the size of the InAs stressor island deepens the confinement potential. To verify this, QD0 PL redshifts measured from InGaAs SIQD samples were plotted as a function of average island height, as presented in Fig. 4.9 (a) with filled rectangles. The data shows clear correlation which is accentuated by the fitted curve (dashed line), drawn as a guide for the eye. The redshift increases with increasing island height but starts to saturate as the height approaches 30 nm. There is a good agreement between the experimental behavior and the strain calculations shown in Fig. 4.5. In Fig. 4.9 (b), the average level splitting of each InGaAs SIQD sample is plotted against stressor height (open circles). A linear fit to the data (dotted line) shows that with increasing island size, the separation between consecutive QD states is reduced. This can be explained by the fact that an increase in the stressor size increases the physical width of the confinement potential, as is seen also in Fig. 4.5.

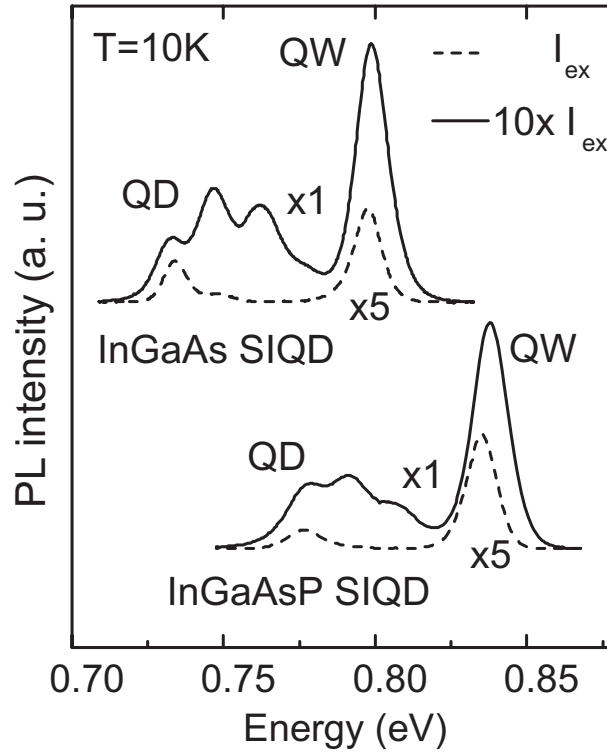


Figure 4.8. PL spectra of InGaAs and InGaAsP SIQD samples measured at low (dashed lines) and high (solid lines) excitation intensity [publ. III].

Furthermore, to study the homogeneity of the quantum dots, the linewidths of the QD PL transitions were extracted from the fitted Gaussian profiles in publication III and compared to the FWHM of the island height distribution from the respective samples. Curiously, little or no correlation between the homogeneity of the stressor islands and the PL linewidth was observed. The FWHM of the QD PL peaks was about the same as the FWHM of the QW PL peak (13–21 meV). These observations and earlier results from InGaAs/GaAs SIQDs [3] indicate that the FWHM of the SIQD ensemble is mainly determined by the QW confinement along the growth (z) axis and no broadening due to inhomogeneity in the lateral confinement is observed. This suggests that the strain fields inducing the QDs are in fact very homogeneous, despite the apparent stressor height inhomogeneity. It was suggested that this behaviour may be linked to the growth thermodynamics. However, the exact mechanism behind the phenomenon and how it relates to the height distribution of the islands remains a topic for further study.

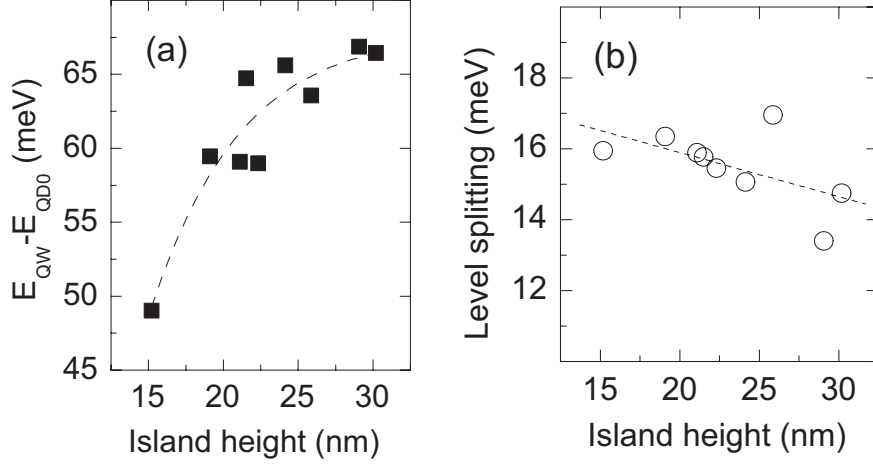


Figure 4.9. (a) Redshift of the QD0 PL peak from the InGaAs QW peak as a function of island height (filled rectangles). The fitted curve (dashed line) is shown as a guide for the eye. (b) Average level splitting of the InGaAs SIQD states as a function of stressor height (open circles). The dotted line is a linear fit to the data [publ. III]

In publication V, the electronic structure and the emission properties of the InGaAs(P)/InP SIQDs were tailored by adjusting the sample structure. First, the ground state emission wavelength was tuned from 1.3 to 1.7 μm by changing the composition of a nearly lattice-matched InGaAsP QW. It was observed that the state structure of the SIQDs, i.e., level splitting and redshift, or the QD PL peak FWHM were not affected significantly even though the QW band gap was varied over a fairly large range ($\Delta E_g \approx 0.25$ eV). The depth of the lateral SIQD confinement potential was adjusted by changing the thickness of the InP capping layer. The cap thickness has an effect on the band-edge modulation because the strain under the island decays as a function of distance to the surface. Fig. 4.10 shows PL spectra from InGaAs/InP SIQD samples with a varying cap thickness. The QD0 PL peak redshift from the QW peak increases by 17 meV (50 to 67 meV) as the capping layer thickness is decreased from 13 to 4 nm. The same effect was also observed by solving the electronic states numerically for the confinement potentials obtained from the strain calculations. Moreover, the PL intensity of the SIQD transitions is seen to diminish as the cap thickness is reduced to 4 nm. On the other hand, the intense PL from

the QW indicates that carriers are able to recombine radiatively in the QW. It was suggested that the carriers in the vicinity of the InAs stressors might be captured into the islands and exhibit pronounced non-radiative recombination.

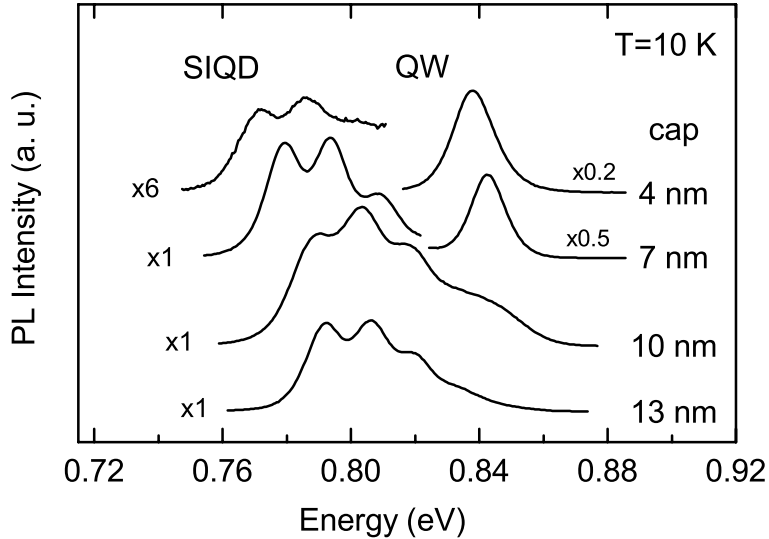


Figure 4.10. PL spectra of InGaAs/InP SIQDs with a varying cap thickness. The curves are offset vertically and the intensity of the QW peaks in the two topmost spectra are scaled down for clarity [publ. V].

In publication VI, carrier dynamics in InGaAsP/InP SIQDs was investigated. The effect of varying the distance between the surface and the QW was studied by time-resolved PL measurements. Rate equations were used to calculate the carrier dynamics. The formulation of the rate equations used for the modeling of SIQDs has been detailed previously [4], and calculations based on the model are in good agreement with the experimental data measured from InGaAs/GaAs SIQD structures. Because holes relax typically much more rapidly than electrons, the hole populations can be assumed to be thermal. Therefore, the temporal behaviour of the PL peaks is governed by the electron populations and the holes can be excluded from the model. Due to surface-related effects, observed here in Fig. 4.10 as diminishing PL intensity with decreasing cap thickness, the rate equation model was augmented to include the effect of the surface processes. A new equation to represent the electron population in the surface states was added. Moreover, transition rate terms from the QW and different QD states to the

surface were also added along with a surface recombination term (including recombination in the InAs islands).

The rate equations used for the carrier concentrations of the QD ($N_{QD,i}$), surface (N_s) and QW (N_W) states are

$$\begin{aligned} \frac{dN_{QD,i}(t)}{dt} = & -\frac{N_{QD,i}(t)}{\tau_{rec,QDi}} + \frac{N_{QD,i+1}(t)}{2\tau_{rel,QD,i+1}} f_i(t) \\ & -\frac{N_{QD,i}(t)}{2\tau_{rel,QD,i}} f_{i-1}(t) + \frac{N_W(t)}{\tau_{cap}} f_i(t) - \frac{N_{QD,i}(t)}{\tau_{D,i \rightarrow s}} f_s(t), \end{aligned} \quad (4.1)$$

$$\frac{dN_s(t)}{dt} = \frac{N_W(t)}{\tau_{W \rightarrow s}} f_s(t) + \frac{N_{QD,i}(t)}{\tau_{D,i \rightarrow s}} f_s(t) - \frac{N_s(t)}{\tau_s}, \quad (4.2)$$

and

$$\frac{dN_W(t)}{dt} = -\frac{N_W(t)}{\tau_{rec,QW}} - \frac{N_W(t)}{\tau_{cap,i}} f_i(t) - \frac{N_W(t)}{\tau_{W \rightarrow s}} f_s(t), \quad (4.3)$$

where $\tau_{cap,i}$ is electron capture time constant for the QW to the QD transition, and τ_{rec} and τ_{rel} are the recombination and relaxation time constants, respectively. QW to surface ($\tau_{W \rightarrow s}$) and QD to surface ($\tau_{D \rightarrow s}$) time constants describe the transition of the QW and QD carriers to the surface while τ_s represents the time constant of surface recombination. State filling factor $f_i(t) = (D_i(t) - N_i(t))$ represents the number of empty states available for transition, and D_i is the density of states.

The effect of the surface processes on the level populations calculated by the rate equation model is shown in Fig. 4.11. The dashed curves are calculated electron populations (proportional to PL intensity) using the parameters of a typical SIQD sample neglecting surface capture. The solid curves are calculated with the same SIQD parameters but taking into account the described surface processes. Due to constraints of the model used, the first 0–1 ns after the excitation pulse have not been simulated. The surface processes are saturated after the excitation pulse. At lower QW carrier densities (starting around 2 ns) the transitions from the QD states to the surface become more prominent. This leads to a decreasing negative slope

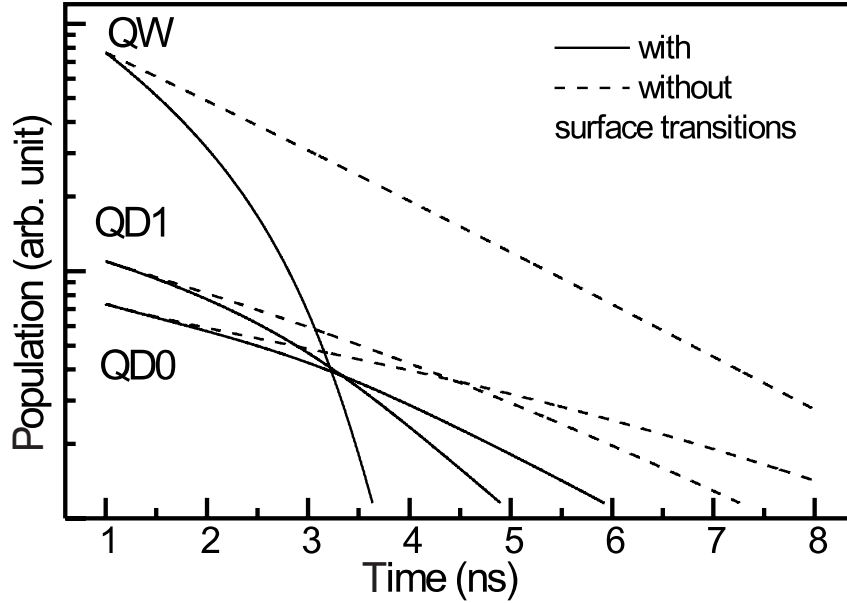


Figure 4.11. QD state and QW populations of a typical InGaAsP/InP SIQD sample as a function of time calculated by the rate equation model with (solid line) and without (dashed line) surface transitions [publ. VI].

of the transient curve with time. The dashed curves (calculated without surface effects) do not exhibit similar behaviour.

The measured TRPL transients from InGaAsP/InP SIQD samples with a cap layer thickness of 7, 10, and 13 nm are shown in Fig. 4.12 (a), (c), and (e), respectively. The corresponding rate equation populations from the QD0, QD1, and QW states are shown in Fig. 4.12 (b), (d), and (f). It is observed that the thinner the cap layer is, the faster the PL intensity decays. The experimental decay times were determined by fitting the exponential profile $Ae^{-\frac{t}{\tau_{dec}}}$ to the QD PL transients, neglecting the first part of each transient where the QW population is high. As the cap thickness is reduced from 13 to 7 nm, $\tau_{dec,QD0}$ decreases from 1.6 to 0.75 ns. This trend can be explained by the increase in electron recombination via surface processes with the decrease in cap thickness.

The rate equation model agrees qualitatively with the measurements. As the distance to the surface is decreased from 13 to 7 nm, the capture probability from the QD states to the surface states increases by a factor of 14. Simultaneously, the capture from the QW to the surface experiences a five-fold increase, suggesting that the capture from the QD states is more

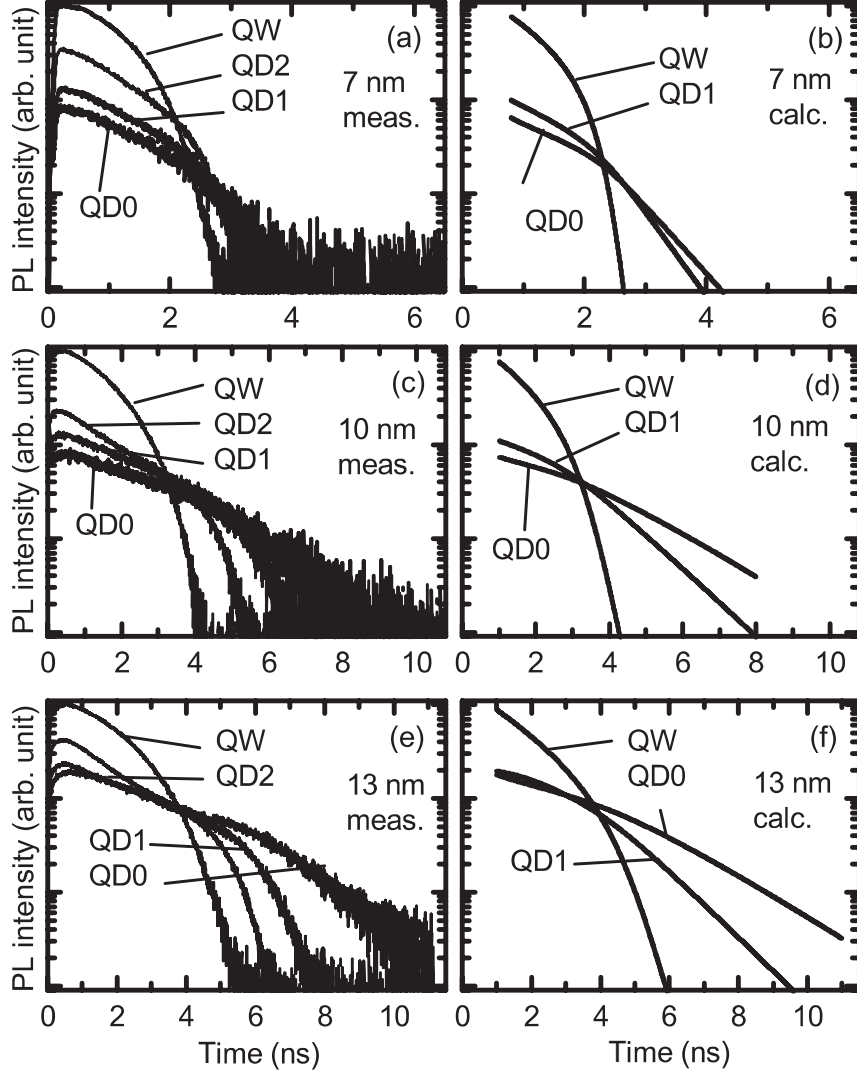


Figure 4.12. TRPL transients from SIQD samples with a cap layer thickness of (a) 7 nm, (c) 10 nm, and (e) 13 nm. PL intensity curves from the QW, QD0, QD1, and QD2 transitions are shown. The corresponding rate equation calculations to TRPL results are shown in (b), (d), and (f) [publ. VI].

pronounced. The position of the QD under the InAs island suggests that the InAs island itself and surface states associated with it capture electrons more effectively than the InAs wetting layer. This would also explain the observation in Fig. 4.10 that, unlike the SIQD luminescence, the QW PL peak is not quenched with decreasing cap thickness.

5 Surface passivation of GaAs by GaN

This chapter discusses the results presented in publications VII and VIII. In these papers, the epitaxial growth of GaN on GaAs, and the passivation of GaAs surface by epitaxial GaN and nitridation were studied.

The high density of surface states in GaAs are known to cause surface Fermi level pinning near the midgap. This can be a limiting factor in the performance of advanced electronic and optoelectronic devices, especially in low-dimensional structures. A variety of different passivation techniques has been studied to solve this problem. GaP formed by As/P exchange reaction, native oxides, standard Si-based insulators (SiO_2 and Si_3N_4), and a variety of plasma nitridation methods, have been demonstrated to passivate GaAs surfaces [88, 89].

Near-surface quantum wells (QWs) have been shown to be an effective means of probing the surface states in GaAs [90]. The coupling between the confined states in the QW with surface states near the band edges is observed as a redshift and intensity decrease of the QW PL peak. Previously, ultrathin InP layers have been shown to be effective in the passivation of AlGaAs/GaAs near-surface QWs [79, 91–93]. In publication VIII it was shown that epitaxial GaN can also be used as a GaAs surface passivation layer. PL intensity enhancements of up to almost three orders of magnitude were observed from InGaAs/GaAs near-surface QWs passivated with GaN.

First, the initial low-temperature growth of cubic GaN on GaAs(100) surface was studied in publication VII. The morphology of the grown layer was found to depend on the growth temperature and the molar flow ratio of group V and III precursors (V/III ratio). DMHy has a lower decomposition temperature than the more commonly used nitrogen precursor ammonia (NH_3), and allows the use of lower growth temperatures without high V/III molar ratios. The moderate growth temperature protects the GaAs

substrate from decomposition by As desorption. The growth temperatures ranged from 550 °C to 700 °C. The GaN layers were grown with V/III ratios between 12.5 – 200 at a growth rate of 2 Å/s.

Figure 5.1 shows atomic force micrographs from four samples with the nominal GaN thickness of 5 nm grown at 550–700 °C with the V/III ratio of 100. Samples grown at 550 and 600 °C show similar morphologies with smooth surfaces and clearly visible monolayer steps. At 650 °C, the morphology is drastically different: The surface is composed of clusters with an approximate base area of $0.5 \times 0.5 \mu\text{m}^2$, an average height of 170 nm and an areal density of $2.2 \times 10^7 \text{cm}^{-2}$. The size of the GaN clusters is increased and the density is correspondingly decreased at 700 °C. By calculating the total volume of the clusters it was seen that virtually all deposited GaN is in the clusters. Thus, the flat region between the clusters is presumably GaAs or nitridated GaAs. It is conceivable that the clustering and the surface deformation are caused by As desorption, and the following partial decomposition of GaAs. As a consequence, a portion of the excess Ga may have recrystallized in the GaN clusters.

Overall, the observed behavior seems to indicate that there is a critical temperature above which the growth of GaN on GaAs is three-dimensional. It was assumed that this is due to a steep decrease in the surface coverage and lifetime of active nitrogen species with the rise in temperature as indicated in Refs. [94] and [95] for MOVPE growth using ammonia. This assumption was supported by the finding that with a V/III ratio of 200, the growth mode remains two-dimensional at 650 °C. A rich DMHy ambient may nitridate the GaAs surface and protect it against decomposition, whereas low V/III ratios would lead to GaAs decomposition and to increased probability for 3D growth of GaN.

The surface passivation effect of the epitaxial GaN was studied in publication VIII. The near-surface QW samples were fabricated by growing a 4-nm-thick $\text{In}_{0.25}\text{Ga}_{0.75}\text{As}$ QW on GaAs, capped by a 5-nm GaAs top barrier. Two different surface passivation methods using DMHy were employed. In the first method, a thin GaN layer (nominally 1-3 ML) was grown at 550 °C on top of the GaAs top barrier. In the second method, the surface of the barrier GaAs layer was nitridated via As-N exchange by switching the TBAs flow to DMHy at 600 °C. After approximately 70 seconds of cooling, the DMHy flow was switched off at 400 °C. For reference, a similar sample was grown without passivation.

The PL spectra of the as-grown unpassivated, nitridated and GaN passivated 4 nm thick $\text{In}_{0.25}\text{Ga}_{0.75}\text{As}/\text{GaAs}$ near-surface QWs with a top barrier

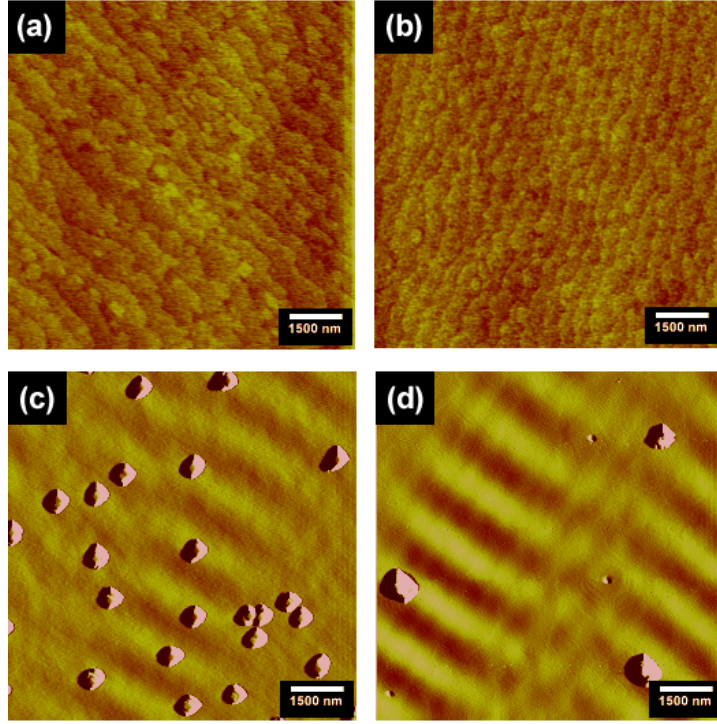


Figure 5.1. Atomic force micrographs ($5 \times 5 \mu\text{m}^2$) taken from GaN samples with a nominal thickness of 5 nm grown on GaAs at (a) 550, (b) 600, (c) 650, and (d) 700 °C. The vertical scale is 3 nm in (a)–(b). Scans (c)–(d) are taken in the AFM deflection mode [publ. VII].

thickness of 5 nm are shown in Fig. 5.2. A deep-QW structure with the top barrier thickness of 20 nm is also shown as a reference. The PL intensity of the GaN passivated sample is enhanced by a factor of 21 compared to the unpassivated QW. For samples stored in ambient air for five months this factor was close to 10^3 (not shown here). A small redshift of 2.8 meV can be seen in the PL spectrum of the GaN passivated quantum well compared to unpassivated structure. This behaviour is probably caused by the formation of $\text{GaAs}_x\text{N}_{1-x}$ in the top barrier GaAs layer due to arsenic-nitrogen exchange. As a consequence, the nominally 5 nm thick top barrier GaAs layer has a graded composition of GaAsN. Thus, the QW barrier height is presumably reduced because with low fractions of nitrogen $\text{GaAs}_x\text{N}_{1-x}$ has a lower band gap than GaAs. This is seen as the redshift of the PL peak. These assumptions are supported by the fact that even a larger redshift (4.9 meV) is evident in the spectrum of $\text{In}_x\text{Ga}_{1-x}\text{As}/\text{GaAs}$ QW passivated with the nitridation method. It can be expected that in the case of nitridation passivation, more GaAsN (with a low band gap) is formed in the top barrier

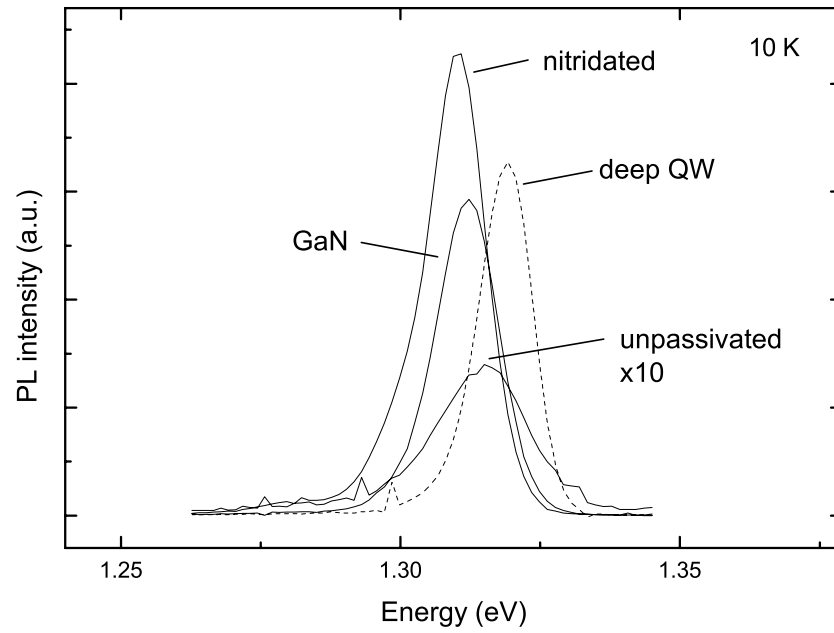


Figure 5.2. PL spectra of as-grown passivated 4 nm thick $\text{In}_{0.25}\text{Ga}_{0.75}\text{As}/\text{GaAs}$ near-surface QWs. The PL intensities of the passivated samples are enhanced and the peaks are slightly red-shifted as compared to the unpassivated QW [publ. VIII].

layer, and the degree of the formation of pure GaN (with a large band gap) is uncertain.

6 Summary

Coherent Stranski-Krastanov growth is widely applied in self-assembled fabrication of semiconductor nanostructures. The growth method can be applied to a number of semiconductor material systems, yielding such potential device applications as quantum dot lasers, all-optical switches, and single-photon light sources. Typically, such QD devices consist of quantum dot islands buried in a barrier material with a higher band gap.

In this thesis, however, MOVPE-grown self-assembled InAs islands on InP were utilized in a different way. On the one hand, InAs islands were transformed into quantum rings. Alternatively, InAs islands were used as stressors to induce quantum dots in a near-surface quantum well. In both cases, the strain of the elastically relaxed InAs island was found to play a major role, either in creating the SIQD confinement, or as the driving force of the dot-to-ring transformation. The structures were characterized by atomic force microscopy and low-temperature PL spectroscopy.

Fabrication of self-assembled semiconductor quantum rings has predominantly relied on the partial capping of islands to induce the dot-to-ring transformation. In this work, the significant change in the morphology was achieved without capping, i.e., simply by annealing as-grown InAs/InP islands in a phosphorus-rich flux. The transformation was explained by As/P exchange and strain-driven migration of In(As)P-like material outward from the top of the elastically relaxed InAs island. With the proposed method, 6–10-nm-high rings with a distinct center hole, and an outer diameter of 250–300 nm were achieved. The rings were found to consist of an undetermined composition of InAsP.

It was also demonstrated that InGaAs(P)/InP strain-induced quantum dots can be realized using InAs stressor islands. To adjust the depth of the strain-induced lateral confinement potential, the height of the islands was tuned from 15 to 30 nm by varying the growth conditions. As/P exchange was found to result in the accumulation of excess material in the InAs

islands, especially at the highest growth temperature of 570 °C. The growth procedure was modified by starting to ramp the growth temperature down a few seconds before the island deposition. This was found to reduce the As/P exchange and improve the uniformity of the islands without affecting the areal island density. Furthermore, the compressively strained near-surface quantum well was found to affect the self-assembly of the InAs islands.

By varying the composition of the nearly-lattice-matched InGaAsP/InP QW, the SIQD ground state emission wavelength was tuned from 1.3 to 1.7 μm . Luminescence from the excited states in the SIQD, having a level splitting of roughly 15 meV was also observed. The redshift of the SIQD ground state transition from the QW PL peak was found to increase up to 67 meV as the distance between the SIQD and the stressor was reduced to 4 nm. Simultaneously, the luminescence intensity of the SIQD peaks was notably reduced. Time-resolved PL measurements revealed that the intensity reduction is accompanied by a faster decay in the carrier populations of the SIQD states.

Finally, the growth of GaN layers for the surface passivation of GaAs was investigated. The passivation effect was probed by PL measurements of near-surface InGaAs/GaAs QWs. The luminescence intensity of GaN passivated samples was clearly enhanced as compared to unpassivated samples, showing that the growth of a thin epitaxial GaN layer is an effective means of *in situ* surface passivation of GaAs.

On the basis of the results presented, a number of further research subjects could be suggested. First, the detailed structural analysis of the fabricated QRs by TEM might give interesting results on the composition of the rings and deepen the understanding of the growth mechanisms. Secondly, the possibility of utilizing SIQDs in optoelectronic device structures, for example in the active region of a QD laser, can be explored. This could prove to be somewhat challenging because it would require sandwiching an SIQD layer without affecting the dots. Thirdly, further investigation of the GaN passivation technique and how it affects the surface electric fields, e.g., by time-resolved PL or other optical means, might be a fruitful research topic. As surface passivation can improve the performance of both electrical and optical semiconductor structures, the research could perhaps open the door to relevant device applications.

References

- [1] P. Michler, A. Kiraz, C. Becher, W. V. Schoenfeld, P. M. Petroff, L. Zhang, E. Hu, and A. Imamoglu, *Science* **290**, 2282 (2000).
- [2] Y. Arakawa and H. Sakaki, *Appl. Phys. Lett.* **40**, 939 (1982).
- [3] H. Lipsanen, M. Sopanen, and J. Ahopelto, *Phys. Rev. B* **51**, 13868 (1995).
- [4] S. Grosse, J. H. H. Sandmann, G. von Plessen, J. Feldmann, H. Lipsanen, M. Sopanen, J. Tulkki, and J. Ahopelto, *Phys. Rev. B* **55**, 4473 (1997).
- [5] J. Tulkki and A. Heinämäki, *Phys. Rev. B* **51**, 8239 (1995).
- [6] A. Lorke, R. J. Luyken, A. O. Govorov, J. P. Kotthaus, J. M. Garcia, and P. M. Petroff, *Phys. Rev. Lett.* **84**, 2223 (2000).
- [7] R. Mueller-Mach, G. O. Mueller, M. R. Krames, and T. Trottier, *Sel. Top. Quantum Electron.* **8**, 339 (2002).
- [8] S. Nakamura, *Sel. Top. Quantum Electron.* **3**, 712 (1997).
- [9] H. Kroemer, *J. Cryst. Growth* **251**, 17 (2003).
- [10] Z. Pan, T. Miyamoto, D. Schlenker, F. Koyama, and K. Iga, *Jpn. J. Appl. Phys.* **38**, 1012 (1999).
- [11] L. Li, B.-K. Han, D. Law, C. H. Li, Q. Fu, and R. F. Hicks, *Appl. Phys. Lett.* **75**, 683 (1999).
- [12] N. Carlsson, T. Junno, L. Montelius, M.-E. Pistol, L. Samuelson, and W. Seifert, *J. Cryst. Growth* **191**, 347 (1998).
- [13] M. E. Heimbuch, A. L. Holmes, Jr., C. M. Reaves, M. P. Mack, S. P. DenBaars, and L. A. Coldren, *J. Electron Mater.* **23**, 87 (1994).

- [14] D. J. Eaglesham and M. Cerullo, *Phys. Rev. Lett.* **64**, 1943 (1990).
- [15] S. Guha, A. Madhukar, and K. C. Rajkumar, *Appl. Phys. Lett.* **57**, 2110 (1990).
- [16] T. R. Ramachandran, R. Heitz, P. Chen, and A. Madhukar, *Appl. Phys. Lett.* **70**, 640 (1997).
- [17] R. Nötzel, J. Temmyo, and T. Tamamura, *Nature* **369**, 131 (1994).
- [18] M. Sopanen, H. Lipsanen, and J. Ahopelto, *Appl. Phys. Lett.* **67**, 3768 (1995).
- [19] A. Ponchet, A. L. Corre, H. L'Haridon, B. Lambert, and S. Salaun, *Appl. Phys. Lett.* **67**, 1850 (1995).
- [20] F. Hatami, N. N. Ledentsov, M. Grundmann, J. Bohrer, F. Heinrichsdorff, M. Beer, D. Bimberg, S. S. Ruvimov, P. Werner, U. Gosele, et al., *Appl. Phys. Lett.* **67**, 656 (1995).
- [21] W. Seifert, N. Carlsson, J. Johansson, M.-E. Pistol, and L. Samuelson, *J. Cryst. Growth* **170**, 39 (1997).
- [22] D. Leonard, M. Krishnamurthy, C. M. Reeves, S. P. Denbaars, and P. M. Petroff, *Appl. Phys. Lett.* **63**, 3203 (1993).
- [23] A. Ponchet, A. L. Corre, H. L'Haridon, B. Lambert, S. Salaun, D. Alquier, D. Lacombe, and L. Durand, *Appl. Surf. Sci.* **123/124**, 751 (1998).
- [24] J. Johansson, N. Carlsson, and W. Seifert, *Physica E* **2**, 667 (1998).
- [25] M. Taskinen, M. Sopanen, H. Lipsanen, J. Tulkki, T. Tuomi, and J. Ahopelto, *Surf. Sci.* **376**, 60 (1997).
- [26] A.-L. Barabasi, *Appl. Phys. Lett.* **70**, 2565 (1997).
- [27] J. Johansson and W. Seifert, *J. Cryst. Growth* **234**, 132 (2002).
- [28] G. Medeiros-Ribeiro, A. M. Bratkovski, T. I. Kamins, D. A. Ohlberg, and R. S. Williams, *Science* **279**, 353 (1998).
- [29] L. G. Wang, P. Kratzer, N. Moll, and M. Scheffler, *Phys. Rev. B* **62**, 1897 (2000).
- [30] G. Medeiros-Ribeiro, *phys. stat. sol. (b)* **230**, 443 (2002).

- [31] J. M. Garcia, J. P. Silveira, and F. Briones, *Appl. Phys. Lett.* **77**, 409 (2000).
- [32] S. Yoon, Y. Moon, T.-W. Lee, E. Yoon, and Y. D. Kim, *Appl. Phys. Lett.* **74**, 2029 (1999).
- [33] M. Borgstrom, J. Johansson, L. Samuelson, and W. Seifert, *Appl. Phys. Lett.* **78**, 1367 (2001).
- [34] C. Paranthoen, N. Bertru, O. Dehaese, A. Le Corre, S. Loualiche, B. Lambert, and G. Patriarche, *Appl. Phys. Lett.* **78**, 1751 (2001).
- [35] P. J. Poole, R. L. Williams, J. Lefebvre, and S. Moisa, *J. Cryst. Growth* **257**, 89 (2003).
- [36] Y. Sakuma, K. Takemoto, S. Hirose, T. Usuki, and N. Yokoyama, *Physica E* **26**, 81 (2005).
- [37] Z. Alferov, *IEEE J. of Selected Topics in Quantum Electronics* **6**, 832 (2000).
- [38] R. Prasanth, J. E. M. Haverkort, A. Deepthy, E. W. Bogaart, J. J. G. M. van der Tol, E. A. Patent, G. Zhao, Q. Gong, P. J. van Veldhoven, R. Nötzel, et al., *Appl. Phys. Lett.* **84**, 4059 (2004).
- [39] I. Kamiya, I. Tanaka, Y. Tada, M. Azuma, K. Uno, and H. Sakaki, *J. Cryst. Growth* **278**, 98 (2005).
- [40] D. Bimberg, M. Kuntz, and M. Laemmlin, *Microelectron. J.* **36**, 175 (2005).
- [41] Y. Aharonov and D. Bohm, *Phys. Rev.* **115**, 485 (1959).
- [42] R. A. Römer and M. E. Raikh, *phys. stat. sol. (b)* **221**, 535 (2000).
- [43] R. Leturcq, L. Schmid, K. Ensslin, Y. Meir, D. C. Driscoll, and A. C. Gossard, *Phys. Rev. Lett.* **95**, 126603 (2005).
- [44] U. F. Keyser, C. Fuhner, S. Borck, R. J. Haug, M. Bichler, G. Abstreiter, and W. Wegscheider, *Phys. Rev. Lett.* **90**, 196601 (2003).
- [45] H. Pettersson, R. J. Warburton, A. Lorke, K. Karrai, J. P. Kotthaus, J. M. Garcia, and P. M. Petroff, *Physica E* **6**, 510 (2000).
- [46] R. J. Warburton, C. Schulhauser, D. Haft, C. Schafflein, K. Karrai, J. M. Garcia, W. Schoenfeld, and P. M. Petroff, *Phys. Rev. B* **65**, 113303 (2002).

- [47] D. Granados, J. M. Garcia, T. Ben, and S. I. Molina, *Appl. Phys. Lett.* **86**, 071918 (2005).
- [48] X. W. Zhang, N. F. Chen, F. Yan, and W. A. Goedel, *Appl. Phys. Lett.* **86**, 203102 (2005).
- [49] J. M. Garcia, G. Medeiros-Ribeiro, K. Schmidt, T. Ngo, J. L. Feng, A. Lorke, J. Kotthaus, and P. M. Petroff, *Appl. Phys. Lett.* **71**, 2014 (1997).
- [50] A. Lorke, R. J. Luyken, J. M. Garcia, and P. M. Petroff, *Japan. J. Appl. Phys.* **40**, 1857 (2001).
- [51] A. Lorke, R. Blossey, J. M. Garcia, M. Bichler, and G. Abstreiter, *Mat. Sci. Eng. B* **88**, 225 (2002).
- [52] R. Blossey and A. Lorke, *Phys. Rev. E* **65**, 021603 (2002).
- [53] D. Granados and J. M. Garcia, *Appl. Phys. Lett.* **82**, 2401 (2003).
- [54] D. Granados and J. M. García, *J. Cryst. Growth* **251**, 213 (2003).
- [55] R. J. Warburton, C. Schäfflein, D. Haft, F. Bickel, A. Lorke, K. Karrai, J. M. Garcia, W. Schoenfeld, and P. M. Petroff, *Physica E* **9**, 124 (2001).
- [56] P. Offermans, P. M. Koenraad, J. H. Wolter, D. Granados, J. M. Garcia, V. M. Fomin, V. N. Gladilin, and J. T. Devreese, *Appl. Phys. Lett.* **87**, 131902 (2005).
- [57] F. Suárez, D. Granados, M. L. Dotor, and J. M. García, *Nanotechnology* **15**, S126 (2004).
- [58] B. C. Lee, O. Voskoboynikov, and C. P. Lee, *Physica E* **24**, 87 (2004).
- [59] T. Raz, D. Ritter, and G. Bahir, *Appl. Phys. Lett.* **82**, 1706 (2003).
- [60] J. Cui, Q. He, X. M. Jiang, Y. L. Fan, X. J. Yang, F. Xue, and Z. M. Jiang, *Appl. Phys. Lett.* **83**, 2907 (2003).
- [61] S. W. Lee, L. J. Chen, P. S. Chen, M.-J. Tsai, C. W. Liu, T. Y. Chien, and C. T. Chia, *Appl. Phys. Lett.* **83**, 5283 (2003).
- [62] S. Kobayashi, C. Jiang, T. Kawazu, and H. Sakaki, *Jpn. J. Appl. Phys.* **43**, L662 (2004).
- [63] T. W. Kim, E. H. Lee, K. H. Lee, J. S. Kim, and H. L. Park, *Appl. Phys. Lett.* **84**, 595 (2004).

- [64] Z. Gong, Z. C. Niu, S. S. Huang, Z. D. Fang, B. Q. Sun, and J. B. Xia, *Appl. Phys. Lett.* **87**, 093116 (2005).
- [65] T. Mano, T. Kuroda, S. Sanguinetti, T. Ochiai, T. Tateno, J. Kim, T. Noda, M. Kawabe, K. Sakoda, G. Kido, et al., *Nano Lett.* **5**, 425 (2005).
- [66] Q. Gong, R. Notzel, P. J. van Veldhoven, T. J. Eijkemans, and J. H. Wolter, *Appl. Phys. Lett.* **84**, 275 (2004).
- [67] Q. Xie, P. Chen, and A. Madhukar, *Appl. Phys. Lett.* **65**, 2051 (1994).
- [68] Y. Kobayashi and N. Kobayashi, *Jpn. J. Appl. Phys.* **31**, 3988 (1992).
- [69] K. Kash, R. Bhat, D. D. Mahoney, P. S. D. Lin, A. Scherer, J. M. Worlock, B. P. V. der Gaag, M. Koza, and P. Grabbe, *Appl. Phys. Lett.* **55**, 681 (1989).
- [70] M. Sopanen, H. Lipsanen, and J. Ahopelto, *Appl. Phys. Lett.* **66**, 2364 (1995).
- [71] W. V. Schoenfeld, T. Lundstrom, P. M. Petroff, and D. Gershoni, *Appl. Phys. Lett.* **74**, 2194 (1999).
- [72] J. Ahopelto, M. Sopanen, and H. Lipsanen, *Jpn. J. Appl. Phys.* **38**, 1081 (1999).
- [73] H. Koskenvaara, T. Hakkarainen, H. Lipsanen, and M. Sopanen, *J. Mat. Sci.* **14**, 357 (2003).
- [74] M. Sopanen, M. Taskinen, H. Lipsanen, and J. Ahopelto, *Appl. Phys. Lett.* **69**, 3393 (1996).
- [75] M. C. Hanna, Z. H. Lu, A. F. Cahill, M. J. Heben, and A. J. Nozik, *J. Cryst. Growth* **174**, 605 (1997).
- [76] T. Wang and A. Forchel, *Appl. Phys. Lett.* **73**, 1847 (1998).
- [77] E. S. Kim, N. Usami, and Y. Shiraki, *Appl. Phys. Lett.* **70**, 295 (1997).
- [78] T. Wang and A. Forchel, *J. Appl. Phys.* **86**, 2001 (1999).
- [79] H. Lipsanen, M. Sopanen, M. Taskinen, J. Tulkki, and J. Ahopelto, *Appl. Phys. Lett.* **68**, 2216 (1996).
- [80] R. Rinaldi, P. V. Giugno, R. Cingolani, H. Lipsanen, M. Sopanen, J. Tulkki, and J. Ahopelto, *Phys. Rev. Lett.* **77**, 342 (1996).

- [81] M. Brasken, M. Lindberg, and J. Tulkki, *Phys. Stat. Sol. A* **164**, 427 (1997).
- [82] M. Brasken, M. Lindberg, M. Sopanen, H. Lipsanen, and J. Tulkki, *Phys. Rev. B* **58**, R15993 (1998).
- [83] C. Lingk, W. Helfer, G. von Plessen, J. Feldmann, K. Stock, M. W. Feise, D. S. Citrin, H. Lipsanen, M. Sopanen, R. Virkkala, et al., *Phys. Rev. B* **62**, 13588 (2000).
- [84] H. Marchand, P. Desjardins, S. Guillon, J.-E. Paultre, Z. Bougrioua, R. Y.-F. Yip, and R. A. Masut, *Appl. Phys. Lett.* **71**, 527 (1997).
- [85] B. Wang, F. Zhao, Y. Peng, Z. Jin, Y. Li, and S. Liu, *Appl. Phys. Lett.* **72**, 2433 (1998).
- [86] H. R. Gutiérrez, M. A. Cotta, J. R. R. Bortoleto, and M. M. G. de Carvalho, *J. Appl. Phys.* **92**, 7523 (2002).
- [87] M. A. Cotta, C. A. C. Mendonca, E. A. Meneses, and M. M. G. Carvalho, *Surf. Sci.* **388**, 84 (1997).
- [88] M. Losurdo, P. Capezzuto, and G. Bruno, *Appl. Phys. Lett.* **81**, 16 (2002).
- [89] S. Anantathanasarn and H. Hasegawa, *Appl. Surf. Sci.* **190**, 343 (2002).
- [90] J. M. Moison, K. Elcess, F. Houzay, J. Y. Marzin, J. M. Gérard, F. Barthe, and M. Bensoussan, *Phys. Rev. B* **41**, 12945 (1990).
- [91] Y. Wada and K. Wada, *Appl. Phys. Lett.* **63**, 379 (1993).
- [92] Y. Wada and K. Wada, *J. Vac. Sci. Technol. B* **12**, 3084 (1994).
- [93] H. Lipsanen, M. Sopanen, J. Ahopelto, J. Sandmann, and J. Feldmann, *Jpn. J. Appl. Phys.* **38**, 1133 (1999).
- [94] S. A. Kukushkin, V. N. Bessolov, A. V. Osipov, and A. V. Luk'yanov, *Phys. Solid State* **43**, 2229 (2001).
- [95] S. W. King, E. P. Carlson, R. J. Therrien, J. A. Christman, R. J. Nemanich, and R. F. Davis, *J. Appl. Phys.* **86**, 5584 (1999).



ISBN 951-22-8037-X
ISBN 951-22-8038-8 (PDF)
ISSN 1795-2239
ISSN 1795-4584 (PDF)